Anonymous Referee #1

The manuscript "Characterization of carbonaceous aerosols in Singapore: insight from black carbon fragments and trace metal ions detected by a soot-particle aerosol mass spectrometer" investigated the sources of carbonaceous aerosol in Singapore by using Positive Matrix Factorization. Besides utilizing the mass spectra of organics, they inserted the mass fragments of rBC and metals in the data matrix in order to improve the interpretation of the aerosol sources in urban area. The authors were able to resolve five sources/types of organic aerosols; hydrocarbon-like OA, oxygenated-HOA, cooking-related OA, less-oxidized oxygenated OA and more-oxidized oxygenated OA.

This paper presents interesting results and novel data analysis methods. Paper is well-written and fluent, and in most parts also easy to understand. It utilizes nicely the whole high resolution mass spectra provided by the SP-AMS, and thoroughly validates the PMF results. However, the interpretation of the PMF factors is sometimes confusing. Additionally, there are shortcomings in the measurement methods, and the authors have drawn some conclusion based on rather weak evidences. Therefore I recommend publication of the manuscript only after the comments below are adequately addressed.

Author's response: We thank for the positive comments from the reviewer. We have provided our point-to-point responses below (in blue colour) to address the questions/comments as shown below:

General comments

The quantitativity of the SP-AMS results is not considered adequately. Since there are several sources of uncertainty in the AMS measurement, e.g. CE, IE and RIE values, the validation of the SP-AMS needs to be done more accurately. Additionally, the weakness of this paper is that only the data from the SP-AMS is utilized. I assume there were also other instruments at the site (for PM, size distribution, BC etc.), or at the air quality monitoring stations nearby, that could be used for the validation/comparison of the SP-AMS data. Without auxiliary data, there accuracy of the given concentrations remains vague.

Author's response: Thanks for the reviewer's suggestion for addressing the SP-AMS measurement uncertainties. In this field study, we conducted four calibrations and obtained an average IE_{NO3} (ionization efficiency of nitrate) value of 7.92e-8 (± 4.08e-09). The standard deviations of RIEs (relative ionization efficiency) for NH_4^+ and rBC have been added in the main text.

The SP-AMS measurements were compared with other co-located measurements from an aethalometer (model AE33, Magee scientific), an OC/EC analyser (Sunset Laboratory) and a Monitor for AeRosols and GAses in ambient air analyzer (MARGA, Metrohm) over the sampling period. Sulfate (SO_4^{2-}) and organic mass concentrations from the SP-AMS (CDCE-corrected) were compared to SO_4^{2-} and OM measured by the MARGA and the OC/EC analyser, respectively (Figure S3a and b in the revised SI). Aside from the good correlations that underline a good temporal response from all instruments, the slopes are in the range of 0.81-0.88, suggesting that the mass concentrations of SO_4^{2-} and organic measured by the SP-AMS are ~12-19% lower than those measured by the MARGA and the OC/EC analyser, respectively. This could be partially explained by the 1 µm cut-size of the SP-AMS, while the two other instruments were measuring $PM_{2.5}$.

The rBC mass concentrations (CE = 0.6) were compared with BC and EC measured by the aethalometer and the OC-EC analyser, respectively (Figure S3c and d in the revised SI). Scatter plots of those comparisons show Pearson coefficients > 0.84, and respective slopes of 0.83 and 1.10, supporting that CE = 0.6 for rBC is a reasonable CE correction approach. Note that no standard approach has been developed for determining CDCE of rBC measured by SP-AMS. As shown in our response to the second reviewer, we determined the CDCE of rBC by comparing BC and EC measured by the aethalometer and the OC/EC analyser, respectively. The median CDCE values ranged between 0.52

and 0.69 as shown in Figure S2 of the revised SI. The following sentences and Figure S3 have been added to the revised manuscript and SI based on the above observations:

Page 2 lines 7-9: "Other co-located instruments for $PM_{2.5}$ characterizations include an aethalometer (AE33, Magee Scientific), a Monitor for Aerosols and Gases (MARGA, Metrohm) and a semi-continuous organic and elemental carbon (OC/EC) analyser (Sunset Laboratory)."

Page 4 lines 27-29: "The campaign averages of RIE_{rBC} and RIE_{NH4} were 0.15 (±0.04) and 4.24 (±0.04), respectively. The default RIE values of nitrate (1.1), sulfate (1.2) and organics (1.4) were used for respective mass concentration quantification (Jimenez, 2003)."

Page 4 lines 33-38: "The SP-AMS measurements were compared with the sulfate and OM concentrations measured by the MARGA and the OC/EC analyser, respectively, showing strong temporal (r = 0.77 and 0.93) and quantitative (slopes = 0.81 and 0.88) agreements between these measurements (Figure S3a and b). A collection efficiency (CE) of 0.6 was used for rBC quantification due to incomplete overlap between the laser vaporizer and the particle beam (Willis et al., 2014). The corrected rBC concentrations were also comparable to those measured by the aethalometer (r = 0.96, slope = 0.83) and the EC measured by the OC/EC analyser (r = 0.84, slope = 1.1) (Figure S3c and d)."

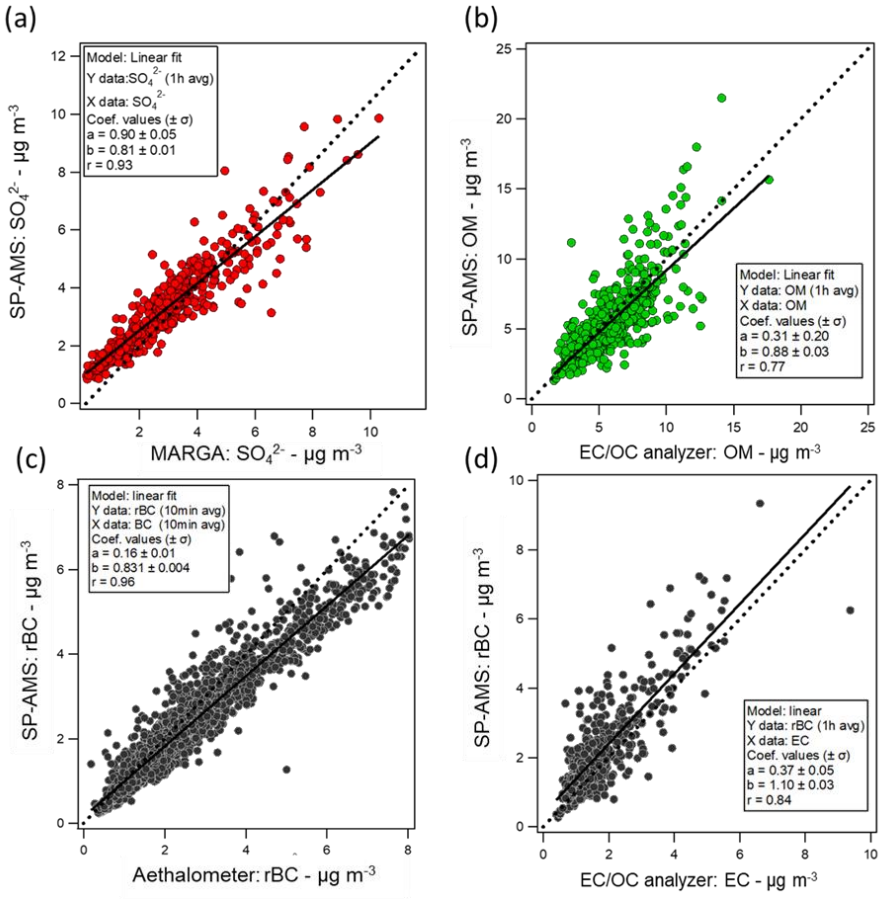

Figure S3: Scatter plots of (a) the hourly-averaged SO_4^{2-} mass concentration measured by the SP-AMS and MARGA, (b) and the hourly-averaged OA and OM (estimated from OC concentration using a 2.2 conversion factor) mass concentrations measured by the SP-AMS and OC/EC analyser, respectively. Comparisons of 10-min averaged rBC mass concentrations measured by the SP-AMS with (c) BC and (d) EC mass concentrations measured by the aethalometer and OC/EC analyser, respectively.

Regarding PMF, I don't understand why only few five metal ions were included in the PMF model even though the SP-AMS can detect quite a few metals. For example, Al, Ca, Cd, Cr, Cu, Fe, Mn, Zn and Sn could be included. I would assume that the inclusion of more metals would improve the interpretation of PMF results. I suggest adding more metals to the PMF analysis because I think that all the interesting information in the data set is not used so far.

Author's response: We agree with the reviewer that it is important to include all the detectable metal signals in the PMF analysis if possible. However, we only reported metals with their average values higher than the limit of detection (Table S2) determined by the particle-free air to ensure the quality of our data analysis. Nickel is a marginal case but a large fraction of its signal remain above its detection limit for investigating the V^+/Ni^+ ratio. To make this point clear, we have revised the sentence in Section 2.3.1 as shown below.

Page 5 lines 24-25: "Lastly, five metal ions (K^+, Na^+, Ni^+, V^+, Rb^+) were included into the PMF model (Figure S4g-i) as the majority of their signals were higher than their respective limit of detection (Table S2)."

In terms of metals, I disagree with the authors that all of the metals presented here can be used as tracers. I agree that Na can come from fuel but it can also originate from other sources in urban areas, for example from coal and biomass burning (e.g. Hsu et al. 2011). Similarly, Rb signal in AMS can originate from coal combustion (Irei et al., 2014). I suggest that the authors consider other sources of metals in urban areas (especially close to industrial areas), and revise their conclusion regarding metals.

Author's response: We agree with the reviewer that most of the metal species that we discussed in the manuscript are not unique tracers. Therefore, our intention is not to discuss how those trace metal species can be used to specify the sources of OA. Rather, we understand that each OA factor identified by the PMF analysis in this work can be originated from different sources. To avoid confusion of our focus in Section 3.5, the sub-heading has been changed to "Characterization of metal ions associated with different OA sources".

With such information, we would like to improve our understanding on the emission characteristics of different OA factors and/or trace metals. For examples, we have pointed out in the manuscript that Na^+ was mainly associated with three OA factors (i.e., HOA, O-HOA, and LO-OOA), which reflects the fact that Na^+ could be emitted from different local combustion sources. Singapore has a biomass clean coal cogeneration plant, but it is important to highlight that natural gas is the major source of electricity (> 95%) in Singapore. Although we didn't observe BBOA factor in this study, we have mentioned that biomass burning can be a possible source of Na^+ in the revised version as suggested by the reviewer. A few sentences in Section 3.5.1 have been revised or added as shown below:

Page 12 lines 5-7: "Based on the PMF results that includes trace metal ions, sodium (Na^+) was mainly associated with HOA, O-HOA and LO-OOA (Figure 5a) that could be due to different types of fossil fuel combustion emissions (e.g., local traffic, shipping, and various industrial activities) as discussed in Section 3.4."

Page 12 lines 20-23: "Biomass burning can be a possible source of Na^+ (Hsu et al., 2011) but no major fresh biomass burning emissions were observed in this study. The MO-OOA factor is suspected to be more influenced by aged regional biomass burning emissions (see more discussion in Section 3.5.2) but Na^+ was not strongly associated with this factor."

Similar to Na^+, we understand that Rb^+ is not a unique tracer for biomass burning. Rather, Rb^+ is likely associated with multiple sources. The results of PMF analysis demonstrated that both K^+ and Rb^+ were mainly associated with MO-OOA (58-66%) followed by the two combustion-related components (HOA and O-HOA). As suggested by the reviewer, we have mentioned that Rb^+ can be a tracer of coal

combustion based on previous studies. Although local coal combustion is uncommon in Singapore, the regional transported of coal combustion plant emissions were still possible. In the revised manuscript, we have revised the discussion to highlight that both regional biomass burning and coal combustion emissions are possible sources of Rb^+. However, it won't substantially change our conclusion that trace metal can allow us to better understand the potential origins of MO-OOA. Since MO-OOA usually represents aged SOA materials in many previous field studies and is a PMF OA factor that cannot provide much mass spectral characteristic for source identification, our data interpretation can provide insight into better identification of MO-OOA sources and/or aging history for other SP-AMS measurements in the future. The majority of Section of 3.5.2 has been rewritten as following.

Page 13, line 1: The sub-heading has been changed to "Potential origins of MO-OOA" to avoid confusion of using Rb^+ as a unique tracer for biomass burning.

Page 13, lines 16-37: "Figures 6c and S14b show that high Rb^+ and K^+ signals were associated with more oxygenated (f_{44} > 0.7) fraction of OA, and moderate correlations between MO-OOA and the two metal were observed (Rb^+, r = 0.58 and K^+, r = 0.71, Figure S13b). Furthermore, the results of PMF analysis demonstrated that both K^+ and Rb^+ were mainly associated with MO-OOA (58-66%, Figure 5a) followed by the two combustion-related components (HOA and O-HOA). Although potassium and rubidium are not unique tracers for a specific combustion source, previous studies have shown that these two metals can be largely associated with biomass burning emissions (Artaxo et al., 1993; Lee et al., 2016; Achad et al., 2018). Note that rubidium has also been used as a coal combustion tracer in previous studies (Fine et al., 2004; Irei et al., 2014). Unlike ambient OA component, the chemical identities of K^+ and Rb^+ are unlikely modified by the oxidative aging of aerosol particles. Therefore, a strong temporal correlation between Rb^+ and K^+ (r = 0.85, Figure 6b) further suggests that they were likely of similar origins in this study.

The regional origin of K^+, Rb^+, $C_2H_4O_2^+$ and MO-OOA were investigated through their PSCF. Their PSCF graphs (Figures 6d and S15a- c) show several common origins with high probability that the highest concentrations could be influenced by biomass burning events from Indonesia (Figure S12a). Nevertheless, coal-fired power plants are located nearby the identified hotspots of Rb^+ and K^+ (Figure S12b) so that a regional transport of coal-fired power plant emissions alongside biomass burning plumes were possible. Note that MO-OOA contributes to the highest fraction of nitrogen-containing organic fragments ($C_xH_yNO_z^+$ ~ 32% and $C_xH_yN^+$ ~ 46%) that can be generated by biomass burning emissions (Mace et al., 2003; Laskin et al., 2009; Desyaterik et al., 2013; Mohr et al., 2013). It is important to point out that most of the previous studies usually describe MO-OOA (or LV-OOA in some earlier studies) as aged SOA component without providing further detail on their potential origin and emission characteristics. Our observations underline the possibility of better understanding the origin of the MO-OOA component through measurements of refractory metals even when atmospheric oxidative processing has made the mass spectral features of aged OA materials less distinguishable."

Specific comments

1. Page 1, Abstract; lines 19-20; "local combustion sources" and "industrial emissions" need to be described in more detailed. What kind of combustion sources, just traffic? What industry there are in that area?

Authors' response: The major industrial activities occurring on Jurong Island (i.e., the large industrial zone in Singapore) have been added in Table S1. Additional locations for some of the industries referred in the table have been added on Figure S1a following the second reviewer's suggestion. The abstract has been modified as follow:

Page 1, lines 21-24: "This work provides evidence that over 90% of rBC was originated from local combustion sources with a major part related to traffic and ~30% of them associated with fresh

secondary organic aerosol (SOA) produced under the influences of shipping and industrial emissions activities (e.g., refineries and petrochemical plants) during daytime."

2. Page 4, line 27; "composition –dependent approach" CE values need to be shown in the paper and the uncertainty of the CE has to be evaluated carefully. Since the RIE for sulfate was not determined, the uncertainty analysis is very important.

Authors' response: The CDCE time series has been added in Figure S2 as shown below. Note that CDCE approach is a well-developed data analysis algorithm for correcting the mass concentrations of NR-PM measured by AMS. To further validate this approach for our dataset, the hourly averaged CDCE-corrected SO_4^{2-} and OM mass concentrations are compared with other co-located measurements of SO_4^{2-} (MARGA) and OM (OC/EC analyser) as shown in Figure S3a and b. The strong agreements between the different measurements were observed as discussed in our responses for the general comments above, suggesting that the CDCE derived for our dataset are reasonably good. The manuscript and SI have been revised accordingly as presented in the responses to the general comments.

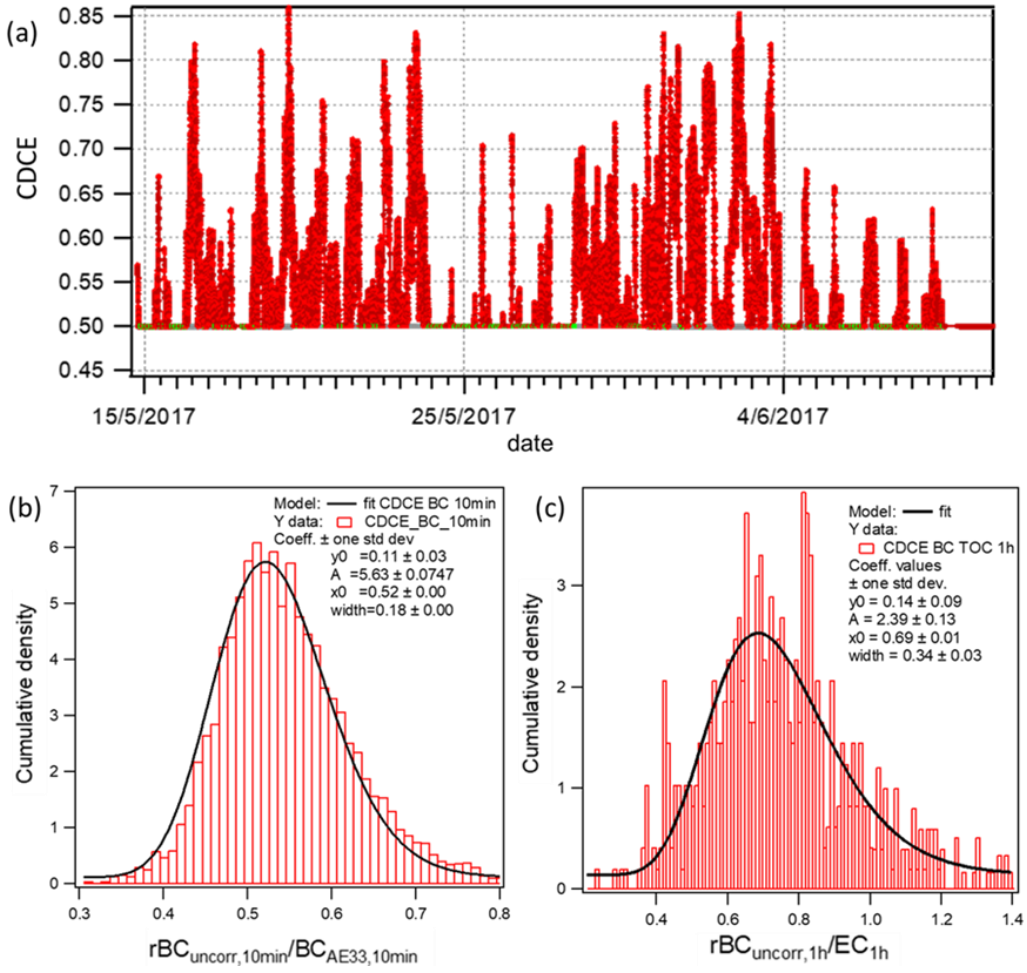

Figure S2: (a) Time series of composition-dependent collection efficiency ($CDCE_{Mid}$) determined over the entire campaign. Cumulative frequency of (b) aethalometer-based CDCE and (c) OC/EC-based CDCE, and their respective lognormal fitting determined over the entire campaign (with the fitting parameters corresponding to the following equation: $Y = y_0 + \mathrm{A}\exp\left\{-\left[\frac{\ln(x/x_0)}{width}\right]^2\right\}$).

3. Page 5, line 13; I don't understand why only few five metal ions were included in the PMF model. I suggest adding more metal ions.

Authors' response: The presence of other metal ions have been investigated in our data analysis but we have decided to exclude those metal ions with signal below the limit of detection. Please refer detail to our response to general comments above.

4. Page 5, line 13-14; metals ions were included in Hz's into the PMF. How does that affect the results of the PMF?

Authors' response: We thank the reviewer for pointing out this. Metal signals in Hz were used for time series comparisons and NWR plots. While for PMF, metal signals were converted to nitrate equivalent mass concentrations assuming their RIE equal to 1. This approach keeps all the signals of organic, C_n^+ and metal fragments within similar order of magnitude. Note that we attempted PMF analysis after applying RIEs on metals – Na^+, Rb^+, V^+, Ni^+ from Carbone et al., (2015) and K^+ from Drewnick et al., (2006) – on the PMF inputs. However, metal signals would drive PMF solutions because of their strong intensities after such RIE correction. Therefore, the RIE of 1 were applied to all metals and the K^+ signals were downweight by a factor 2 for the final PMF solution. To make sure such information clearly delivered in the manuscript, the following sentences have been revised or added in the revised version.

Page 5 lines 2-3: "The signals of these trace metal ions were not calibrated and thus their raw signals were used for investigating their temporal variations."

Page 5 lines 24-27: "Lastly, five metal ions (K^+, Na^+, Ni^+, V^+, Rb^+) were included into the PMF model (Figure S4g-i) as the majority of their signals were higher than their respective limit of detection (Table S2). The metal ion signals were corrected to nitrate equivalent mass concentrations by assuming their RIE values equal to 1 and the K^+ signals were downweight by a factor 2"

5. Page 5, line 30; sulfate increase starting from 10:00 can be explained by the active photochemistry. Could you add a diurnal plot showing solar radiation and sulfate in the same figure?

Authors' response: We have added the diurnal variation of solar radiation to Figure 1c to emphasize the hours of day with intense photochemistry as suggested by the reviewer.

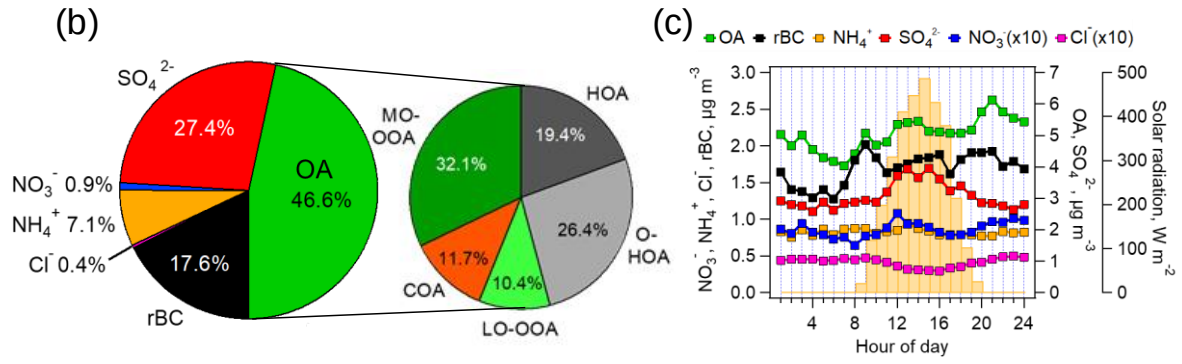

Figure 1: […] (b) Average chemical compositions of NR-PM and rBC with the contribution of the PMF factors to total OA. (c) Diurnal patterns of rBC, total OA, inorganic species and solar radiations (represented by the yellow bars).

6. Page 5, line 30; NH4 ratio and acidity; the discussion on acidity is somewhat unreliable because the RIE for sulfate was not measured. For example in Fig. S4a, it's hard to understand why all the points are below 1:1 line. To me, this seems to be due to the incorrect RIE for sulfate. Could you comment on that?

Authors' response: Regarding the accuracy of SO_4^{2-} mass concentration, we have discussed in our response to the general comments above and we could conclude that the RIE applied for sulfate are reasonable. Note that the main purpose of showing the ratios between measured and predicted NH_4^+ (Figure S6a-c) is to highlight the relative changes in aerosols acidity especially when the high SO_4^{2-} loadings were observed. This relative observation should not be affected by the absolute SO_4^{2-} mass concentrations. Furthermore, previous studies have reported that fine particles encountered in Singapore and Southeast Asia are usually acidic (Budisulistiorini et al., 2018; Pye et al., 2019). Budisulistiorini et al., (2018) recently reported an average $NH_{4,meas}/NH_{4,pred}$ ratio of 0.7 (±0.3) underlining the acidic nature of aerosols outside of hazy periods. Indeed, ammonia emissions caused by biomass burning results in a neutralization of inorganic particles (Budisulistiorini et al., 2018), while usual ammonia level in Singapore remain relatively low compare to other region of the world (Behera et al., 2013).

7. Page 7, line 5; industrial emission; be more specific what kind of emissions

Authors' response: It is rather difficult for us to pin point the exact types of industrial emissions. However, we know that refineries, petrochemical industries and shipping emissions are some of the key emission sources from the industrial zone as reported in Table S1. The sentence has been revised as following.

Page 7 lines 27-29: "It is important to note that the period with elevated concentrations of sulfate and sulfur-containing fragments were synchronized with the sea breeze from the southwest, from which refineries, petrochemical industries and shipping emissions could be carried to our sampling site (Figure 2 and S6e)."

8. Page 7, line 28; define POA, is it only HOA? Isn't COA also primary?

Authors' response: Both HOA and COA are primary in nature. The focus of Section 3.3.1 is combustion emissions, COA are discussed in Section 3.3.2. To avoid such confusion, a sentence has been added at the beginning of Section 3.3.2 to highlight that COA are also one of the major POA component.

Page 9 line 11: "COA is another major POA component identified in this study."

9. Page 7, line 38; "large combustion sources during nighttime" needs to be elaborated since it has such a large effect on diurnal cycle of HOA

Authors' response: We agree with the reviewer that the unknown combustion sources can have substantial impact to the diurnal cycle of HOA. However, their influences were occasionally observed within our sampling period as highlighted in our original discussion. It is difficult to identify the exact emission sources but the elevated concentrations were observed at low wind speed condition, suggesting that they were likely due to local emissions from the city. We do believe it can be related to the local industrial emission, such as the flaring emissions from petrochemical industries. The related text have been revised as following to give the reader some ideas about the potential night time combustion sources.

Page 8 lines 24-35: “High concentrations of rBC, NO_x and HOA were observed during the mid-night between May 25th and 28th, indicating the presence of large combustion sources during nighttime that might impact the air quality at our sampling site occasionally (Figure 1a). This observation also reflected from the diurnal plots (Figures 3 and S8) that the mean mass concentrations of HOA, rBC, NO_X and CO during the mid-night were much higher than their corresponding median values. Figure S8a shows that the highest N:C ratio was observed during the morning traffic peak hours but remained relatively low for the rest of the period. Such observation suggests that the emission characteristics of these unknown combustion sources at nighttime could be different to those associated with traffic emissions during the daytime. Although it is difficult to confirm the origin of those nighttime combustion emissions without further evidence, the observed events were coupled to low wind speed condition, suggesting that they were likely due to local emissions from the city. For example, significant emissions due to flaring from petrochemical industries, which largely depends on plant operation, during the relatively stagnant atmospheric condition could lead to elevated concentrations of the combustion-related species.”

10. Page 9, lines 11-15; “organo-nitrate and nitrogen-containing fragments increased during the daytime in this field study.” Why there is not more discussion on these species if they were detected? What is their contribution to OA or LO-OOA? Add the ratio of N to C (and S:C) to Figure 3.

Authors’ response: N:C ratios have been added to Figure 3 for each factor in the revised version. As shown in the figure below (submitted for Kasthuriarachchi et al., (2020)), nitrogen fragments can be originated from different sources. Since we don’t have strong evidence to develop conclusive arguments regarding the nitrogen compounds chemistry from primary emissions and secondary aerosol formation, we have decided to added/revised a few sentences throughout the manuscript to briefly highlight how nitrogen fragments may be associated with different emissions. Given that the contribution of nitrogen-containing fragments were only ranged from 0.6 to 1.4 % for each PMF OA factor, adding detail discussion for nitrogen-containing fragments may dilute the focus of this manuscript.

Page 8 lines 28-31: Discussion for HOA - “Figure S8a shows that the highest N:C ratio was observed during the morning traffic peak hours but remained relatively low for the rest of the period. Such observation suggests that the emission characteristics of these unknown combustion sources at nighttime could be different to those associated with traffic emissions during the daytime.”

Page 10 line 10-15: Discussion for LO-OOA - “Furthermore, Kasthuriarachchi et al. (2020) reported that the concentrations of organo-nitrate and nitrogen-containing fragments (i.e., $C_xH_yN^+$ and $C_xH_yNO_z^+$) slightly increased during daytime (e.g., Figure S8a) with LO-OOA, contributing to 30% of observed $C_xH_yNO_z^+$ fragments (Figure S10). This suggests that photo-oxidation of VOCs under high-NO_X condition could be a potential pathway toward LO-OOA formation given that the NO_X concentrations reached up to 160 ppb (Figure 1a, mean = 16.5 ppb) during the campaign.”

Page 13, lines 30-32: Discussion for MO-OOA - “Note that MO-OOA contributes to the highest fraction of nitrogen-containing organic fragments ($C_xH_yNO_z^+$ ~ 32% and $C_xH_yN^+$ ~ 46%) that can be generated by biomass burning emissions (Mace et al., 2003; Laskin et al., 2009; Desyaterik et al., 2013; Mohr et al., 2013).”

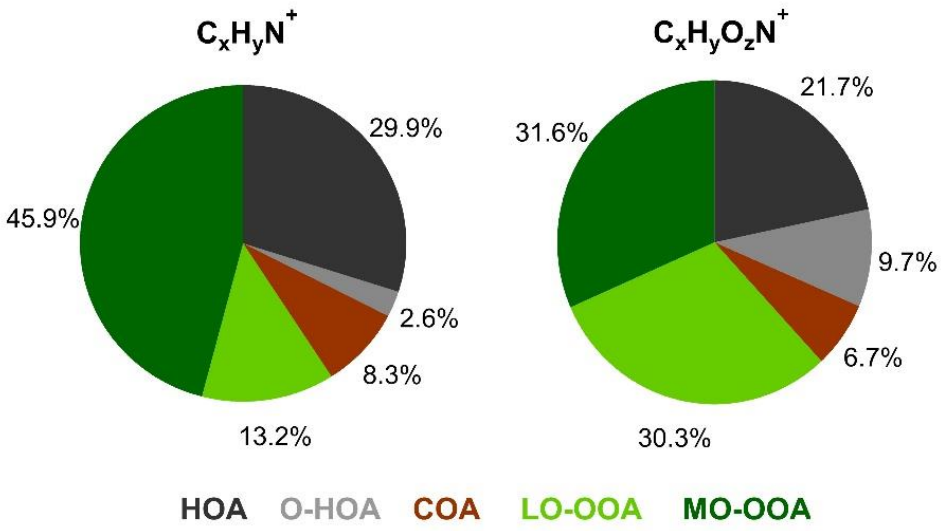

Figure S10: Contributions of each OA factor to the N-containing fragment groups (Kasthuriarachchi et al., (2020)).

11. Page 11, line 5-; Na as a tracer for fossil fuel combustion. Revise this section by taking into account other sources of Na in urban areas (see general comments).

Authors' response: As shown in our responses in the general comments, our intention is not to use Na^+ as a fossil fuel combustion tracer. Rather, we understand that Na^+ can be originated from various sources in urban. In particular, we pointed out that Na^+ was mainly associated with three OA factors (i.e., HOA, O-HOA, and LO-OOA), which reflects the fact that Na^+ could be emitted from different local combustion sources. In addition, although we didn't observe BBOA factor in this study, we have mentioned that biomass burning can be a possible urban source of Na^+ in general in the revised version as suggested by the reviewer. A few sentences in Section 3.5.1 have been revised or added as shown below:

Page 12 lines 5-7: "Based on the PMF results that includes trace metal ions, sodium (Na^+) was mainly associated with HOA, O-HOA and LO-OOA (Figure 5a) that could be due to different types of fossil fuel combustion emissions (e.g., local traffic, shipping, and various industrial activities) as discussed in Section 3.4."

Page 12 lines 20-23: "Biomass burning can be a possible source of Na^+ (Hsu et al., 2011) but no major fresh biomass burning emissions were observed in this study. The MO-OOA factor is suspected to be more influenced by aged regional biomass burning emissions (see more discussion in Section 3.5.2) but Na^+ was not strongly associated with this factor."

12. Page 11, Biomass burning tracers, I don't understand why the contribution of biomass burning has been investigated so extensively even though it does not show up in PMF and the metals are not very good tracers for it. Consider making Section 3.5.2. more compact.

Authors' response: The *m/z* 60 (or $C_2H_4O_2^+$ organic fragments) has been widely used as a tracer organic fragment for identifying BBOA in the PMF analysis. Cubison et al. (2011) have generalized observations from worldwide field data that *m/z* 60 signature become less and less significant in aged BBOA materials. The implication of such observation is that atmospheric aging of BBOA can lead to formation of MO-OOA (or LV-OOA in earlier studies) but their origins cannot be easily identified in

the conventional PMF analysis. Note that MO-OOA usually represents aged SOA materials in many previous field studies and is a common OA factor that cannot provide much mass spectral characteristic for source identification. How we can better understand the origin of MO-OOA is certainly an important research topic for the atmospheric science/chemistry community.

Since biomass burning emissions are commonly observed in the Southeast Asian in general (not within Singapore), we would like to examine if the regional pollutions, such as aged biomass burning and other anthropogenic emissions, may contribute to the observed MO-OOA in this study. This type of investigation is further motivated by our observation that the $f_{C2H4O2+}$ value of MO-OOA is slightly higher than the background value reported in Cubison et al. (2011) and its moderate correlation with K^+ and Rb^+. Although the metal ions that we used in this study are not unique for any specific sources, they are more persistent to atmospheric aging compared to their co-emitted OA materials, and thus can provide insight into the potential sources and/or aging history of MO-OOA. As pointed out by the reviewer in the general comment, we have revised the discussion to highlight the fact that K^+ and Rb^+ can be emitted by both coal combustion and biomass burning. However, it won't substantially change our conclusion that trace metal may allow us to better understand the potential origins of MO-OOA. We do believe the similar approach can also be applied for other SP-AMS measurements in the future.

Since our interested is not limited to the potential influences of aged regional BBOA, we have changed the sub-heading of Section of 3.5.2 to "Potential origins of MO-OOA" in order avoid confusion. Furthermore, the majority of Section 3.5.2 and Section 4 have been rewritten as following,

Section 3.5.2: Page 13, lines 16-37: "Figures 6c and S14b show that high Rb^+ and K^+ signals were associated with more oxygenated (f_{44} > 0.7) fraction of OA, and moderate correlations between MO-OOA and the two metal were observed (Rb^+, r = 0.58 and K^+, r = 0.71, Figure S13b). Furthermore, the results of PMF analysis demonstrated that both K^+ and Rb^+ were mainly associated with MO-OOA (58-66%, Figure 5a) followed by the two combustion-related components (HOA and O-HOA). Although potassium and rubidium are not unique tracers for a specific combustion source, previous studies have shown that these two metals can be largely associated with biomass burning emissions (Artaxo et al., 1993; Lee et al., 2016; Achad et al., 2018). Note that rubidium has been used as a coal combustion tracer in previous studies (Fine et al., 2004; Irei et al., 2014). Unlike ambient OA component, the chemical identities of K^+ and Rb^+ are unlikely modified by the oxidative aging of aerosol particles. Therefore, a strong temporal correlation between Rb^+ and K^+ (r = 0.85, Figure 6b) further suggests that they were likely of similar origins in this study.

The regional origin of K^+, Rb^+, $C_2H_4O_2^+$ and MO-OOA were investigated through their PSCF. Their PSCF graphs (Figures 6d and S15a- c) show several common origins with high probability that the highest concentrations could be influenced by biomass burning events from Indonesia (Figure S12a). Nevertheless, coal-fired power plants are located nearby the identified hotspots of Rb^+ and K^+ (Figure S12b) so that a regional transport of coal-fired power plant emissions alongside biomass burning plumes were possible. Note that MO-OOA contributes to the highest fraction of nitrogen-containing organic fragments ($C_xH_yNO_z^+$ ~ 32% and $C_xH_yN^+$ ~ 46%) that can be generated by biomass burning emissions (Mace et al., 2003; Laskin et al., 2009; Desyaterik et al., 2013; Mohr et al., 2013). It is important to point out that most of the previous studies usually describe MO-OOA (or LV-OOA in some earlier studies) as aged SOA component without providing further detail on their potential origin and emission characteristics. Our observations underline the possibility of better understanding the origin of the MO-OOA component through measurements of refractory metals even when atmospheric oxidative processing has made the mass spectral features of aged OA materials less distinguishable."

Section 4: Page 14, Lines 24-36: "One of the major challenges in interpreting the PMF results from AMS measurements is to identify the origin and aging history of ambient particles associated with highly oxidized OA components (e.g., MO-OOA in this work), as the mass spectral characteristics of OA converge along with their degree of oxidative aging. In general, the relative intensities of some highly oxygenated fragments (e.g. CO^+ and CO_2^+) increase continuously while other mass spectral

features (e.g. alkane/alkene patterns from combustion sources) being diminished during the aging processes. Ng et al., (2010) have visualized such phenomena for SOA components on the f_{43}-f_{44} space. Furthermore, the *m/z* 60 (or $C_2H_4O_2^+$ organic fragments) has been widely used as a tracer ions for BBOA. Cubison et al. (2011) have generalized observations from worldwide field data that *m/z* 60 signature become less and less significant in aged BBOA materials. In this study, we proposed that the MO-OOA component represented aged OA materials impacted by the regional biomass burning and perhaps coal combustion emissions as MO-OOA was associated with refractory K^+ and Rb^+. Given the fact that MO-OOA was the major OA components of the total OA (~32%), this result highlights the fact that the regional pollution can affect the air quality in Singapore even though fresh regional biomass burning episodes were not observed during the sampling period."

13. Page 12, line 24-26; "Kasthuriarachchi et al., (2019) also found that MO-OOA was the major contributor to the observed nitrogen-containing organic fragments that could be largely generated by biomass burning emissions" is contradictory to page 9: "Kasthuriarachchi et al. (2019) reported that the concentrations of organo-nitrate and nitrogen-containing fragments (i.e., CxHyN+ and CxHyNOz+) increased during the daytime in this field study, suggesting that photo oxidation of VOCs under high-NO_X condition could be another potential pathway toward LO-OOA formation". Please revise the sentence/sentences.

Authors' response: The elevated concentrations/signals of LO-OOA factor, $C_xH_yN^+$ and, $C_xH_yNO_z^+$ were observed during the daytime, suggesting that the formation of LO-OOA could result from VOCs photo-oxidation under-high NO_x condition. As shown in the response of comment #10, approximately 13-30% of nitrogen-containing fragments were associated with the LO-OOA factor, whereas MO-OOA accounts for ~50% of nitrogen-containing fragments. The first statement is focusing on the diurnal dynamic and the second statement is about the major contributors of those fragments so that they are not contradict to each other. Note that there were no distinct diurnal pattern for MO-OOA factor. The related sentences were slightly modified as following:

Page 10 line 10-15: Discussion for LO-OOA - "Furthermore, Kasthuriarachchi et al. (2020) reported that the concentrations of organo-nitrate and nitrogen-containing fragments (i.e., $C_xH_yN^+$ and $C_xH_yNO_z^+$) slightly increased during daytime (e.g., Figure S8a) with LO-OOA, contributing to 30% of observed $C_xH_yNO_z^+$ fragments (Figure S10). This suggests that photo-oxidation of VOCs under high-NO_X condition could be a potential pathway toward LO-OOA formation given that the NO_X concentrations reached up to 160 ppb (Figure 1a, mean = 16.5 ppb) during the campaign."

Page 13, lines 30-32: Discussion for MO-OOA - "Note that MO-OOA contributes to the highest fraction of nitrogen-containing organic fragments ($C_xH_yNO_z^+$ ~ 32% and $C_xH_yN^+$ ~ 46%) that can be generated by biomass burning emissions (Mace et al., 2003; Laskin et al., 2009; Desyaterik et al., 2013; Mohr et al., 2013)."

14. Page 12, line 31-33 and Fig. S11, Fig. S11 is confusing. It is very difficult to see which trajectories really pass the two fires shown by the MODIS. Could you just select the trajectory for the peak concentrations of m/z 60? Where are the large urban areas in the map? Do the trajectories pass large cities as well? Is it possible that biomass burning emissions were mixed with urban emissions (that increased Rb and maybe also K)? Please add cities to the map. Why Fig. S11(b) and Fig S11(c) are not on the same scale? Now it is difficult to compare (b) and (c). Add lines between markers to m/z 60 and Rb in Fig. S11a.

Author's response: We agree with the reviewer's comment and have decided to remove this figure in the revised version. Instead, we have added a map of all active fires that occurred over the region during the entire campaign (Figure S12a) with the name of large urban areas. As discussed in our above responses for general comments, we are trying to investigate the potential origins of MO-OOA due to the regional emissions based on its moderate correlation with K^+, Rb^+ and $C_2H_4O_2^+$. Since we

understand that there should be multiple sources of MO-OOA that could be produced from aging of different types of primary and secondary emissions. In the revised manuscript, we would like to highlight the possibilities that regional biomass burning and coal combustion emissions could be linked to the MO-OOA formation. The following text has been added in the manuscript.

Page 13, lines 26-30: "The regional origin of K^+, Rb^+, $C_2H_4O_2^+$ and MO-OOA were investigated through their PSCF. Their PSCF graphs (Figures 6d and S15a- c) show several common origins with high probability that the highest concentrations could be influenced by biomass burning events from Indonesia (Figure S12a). Nevertheless, coal-fired power plants are located nearby the identified hotspots of Rb^+ and K^+ (Figure S12b) so that a regional transport of coal-fired power plant emissions alongside biomass burning plumes were possible."

15. Page 13, lines 21-23; "Furthermore, Na^+ measured by the SP-AMS can potentially be useful for separating rBC from traffic and biomass burning combustion emissions, which required further investigation." I suggest revising this sentence as the evidences provided by this study are not convincing enough. I think that there are multiple sources for Na in urban areas that should be taken into account.

Author's response: As discussed above, we have revised our discussion regarding Na^+. This sentence has been removed in the revised version.

16. Page 13, lines 36-37; "This observation suggest that, in the region, both K+ and Rb+ might be more appropriate tracers for the identification of aged biomass burning than m/z 60." I suggest revising this sentence as Rb may also come from other sources.

Author's response: As discussed above, we have revised our discussion regarding K^+ and Rb^+. This sentence has been removed from the revised conclusion.

Technical corrections:

1. Page 7, line 13; less-oxidized oxygenated OA (LO-OOA)

Author's response: The sentence has been revised accordingly.

2. Supplemental material, could you add a figure showing the contribution of metals to each PMF factor? It would be interesting to see how metals divide between the factors.

Author's response: The figure showing the contribution of metals to each PMF factor is presented in Figure 5a. (Figure 5d in the original version of manuscript).

References

Hsu, L. J., Alwahabi, Z. T., Nathan, G. J., Li, Y., Z. LI, S., Aldén, M.(2011). Sodium and Potassium Released from Burning Particles of Brown Coal and PineWood in a Laminar Premixed Methane Flame Using Quantitative Laser-Induced Breakdown Spectroscopy. Applied spectroscopy, 65, 684-91.

Irei, S., Shimono, A., Hikida, T., Kuramoto, K., Suzuki, Y., Takami, A. (2014). Qualitative Evaluation of m/z 85, 87, and 133 Signals in Organic Aerosol Mass Spectra of Fly Ash Produced by Coal Combustion. Aerosol and Air Quality Research, 14: 406–412.

Author's references:

Achad, M., Caumo, S., de Castro Vasconcellos, P., Bajano, H., Gómez, D. and Smichowski, P.: Chemical markers of biomass burning: Determination of levoglucosan, and potassium in size-classified atmospheric aerosols collected in Buenos Aires, Argentina by different analytical techniques, Microchem. J., 139, 181–187, doi:10.1016/j.microc.2018.02.016, 2018.

Artaxo, P., Gerab, F. and Rabello, M. L.: Elemental composition of aerosol particles from two atmospheric monitoring stations in the Amazon Basin, Nucl. Instrum. Methods Phys. Res. Sect. B Beam Interact. Mater. At., 75(1–4), 277–281, 1993.

Behera, S. N., Betha, R. and Balasubramanian, R.: Insights into Chemical Coupling among Acidic Gases, Ammonia and Secondary Inorganic Aerosols, Aerosol Air Qual. Res., 13(4), 1282–1296, doi:10.4209/aaqr.2012.11.0328, 2013.

Budisulistiorini, S. H., Riva, M., Williams, M., Miyakawa, T., Chen, J., Itoh, M., Surratt, J. D. and Kuwata, M.: Dominant contribution of oxygenated organic aerosol to haze particles from real-time observation in Singapore during an Indonesian wildfire event in 2015, Atmospheric Chem. Phys., 18(22), 16481–16498, doi:https://doi.org/10.5194/acp-18-16481-2018, 2018.

Carbone, S., Onasch, T., Saarikoski, S., Timonen, H., Saarnio, K., Sueper, D., Rönkkö, T., Pirjola, L., Häyrinen, A., Worsnop, D. and Hillamo, R.: Characterization of trace metals on soot aerosol particles with the SP-AMS: detection and quantification, Atmos Meas Tech, 8(11), 4803–4815, doi:10.5194/amt-8-4803-2015, 2015.

Cubison, M. J., Ortega, A. M., Hayes, P. L., Farmer, D. K., Day, D., Lechner, M. J., Brune, W. H., Apel, E., Diskin, G. S., Fisher, J. A., Fuelberg, H. E., Hecobian, A., Knapp, D. J., Mikoviny, T., Riemer, D., Sachse, G. W., Sessions, W., Weber, R. J., Weinheimer, A. J., Wisthaler, A. and Jimenez, J. L.: Effects of aging on organic aerosol from open biomass burning smoke in aircraft and laboratory studies, Atmos Chem Phys, 11(23), 12049–12064, doi:10.5194/acp-11-12049-2011, 2011.

Desyaterik, Y., Sun, Y., Shen, X., Lee, T., Wang, X., Wang, T. and Collett, J. L.: Speciation of "brown" carbon in cloud water impacted by agricultural biomass burning in eastern China, J. Geophys. Res. Atmospheres, 118(13), 7389–7399, doi:10.1002/jgrd.50561, 2013.

Drewnick, F., Hings, S. S., Curtius, J., Eerdekens, G. and Williams, J.: Measurement of fine particulate and gas-phase species during the New Year's fireworks 2005 in Mainz, Germany, Atmos. Environ., 40(23), 4316–4327, doi:10.1016/j.atmosenv.2006.03.040, 2006.

Fine, P. M., Cass, G. R. and Simoneit, B. R. T.: Chemical Characterization of Fine Particle Emissions from the Wood Stove Combustion of Prevalent United States Tree Species, Environ. Eng. Sci., 21(6), 705–721, doi:10.1089/ees.2004.21.705, 2004.

Hsu, L.-J., Alwahabi, Z. T., Nathan, G. J., Li, Y., Li, Z. S. and Aldén, M.: Sodium and Potassium Released from Burning Particles of Brown Coal and Pine Wood in a Laminar Premixed Methane Flame Using Quantitative Laser-Induced Breakdown Spectroscopy:, Appl. Spectrosc., doi:10.1366/10-06108, 2011.

Irei, S., Shimono, A., Hikida, T., Kuramoto, K., Suzuki, Y. and Takami, A.: Qualitative Evaluation of m/z 85, 87, and 133 Signals in Organic Aerosol Mass Spectra of Fly Ash Produced by Coal Combustion, Aerosol Air Qual. Res., 14(1), 406–412, doi:10.4209/aaqr.2013.04.0126, 2014.

Jimenez, J. L.: Ambient aerosol sampling using the Aerodyne Aerosol Mass Spectrometer, J. Geophys. Res., 108(D7), doi:10.1029/2001JD001213, 2003.

Kasthuriarachchi, N. Y., Rivellini, L.-H., Adam, M. G. and Lee, A. K. Y.: Strongly absorptive primary and secondary brown carbon in an urban, under review, Environ Sci Technol, 2020.

Laskin, A., Smith, J. S. and Laskin, J.: Molecular Characterization of Nitrogen-Containing Organic Compounds in Biomass Burning Aerosols Using High-Resolution Mass Spectrometry, Environ. Sci. Technol., 43(10), 3764–3771, doi:10.1021/es803456n, 2009.

Lee, A. K. Y., Willis, M. D., Healy, R. M., Wang, J. M., Jeong, C.-H., Wenger, J. C., Evans, G. J. and Abbatt, J. P. D.: Single-particle characterization of biomass burning organic aerosol (BBOA): evidence for non-uniform mixing of high molecular weight organics and potassium, Atmos Chem Phys, 16(9), 5561–5572, doi:10.5194/acp-16-5561-2016, 2016.

Mace, K. A., Artaxo, P. and Duce, R. A.: Water-soluble organic nitrogen in Amazon Basin aerosols during the dry (biomass burning) and wet seasons, J. Geophys. Res. Atmospheres, 108(D16), doi:10.1029/2003JD003557, 2003.

Mohr, C., Lopez-Hilfiker, F. D., Zotter, P., Prévôt, A. S. H., Xu, L., Ng, N. L., Herndon, S. C., Williams, L. R., Franklin, J. P., Zahniser, M. S., Worsnop, D. R., Knighton, W. B., Aiken, A. C., Gorkowski, K. J., Dubey, M. K., Allan, J. D. and Thornton, J. A.: Contribution of Nitrated Phenols to Wood Burning Brown Carbon Light Absorption in Detling, United Kingdom during Winter Time, Environ. Sci. Technol., 47(12), 6316–6324, doi:10.1021/es400683v, 2013.

Ng, N. L., Canagaratna, M. R., Zhang, Q., Jimenez, J. L., Tian, J., Ulbrich, I. M., Kroll, J. H., Docherty, K. S., Chhabra, P. S., Bahreini, R., Murphy, S. M., Seinfeld, J. H., Hildebrandt, L., Donahue, N. M., DeCarlo, P. F., Lanz, V. A., Prévôt, A. S. H., Dinar, E., Rudich, Y. and Worsnop, D. R.: Organic aerosol components observed in Northern Hemispheric datasets from Aerosol Mass Spectrometry, Atmos Chem Phys, 10(10), 4625–4641, doi:10.5194/acp-10-4625-2010, 2010.

Pye, H. O. T., Nenes, A., Alexander, B., Ault, A. P., Barth, M. C., Clegg, S. L., Collett Jr., J. L., Fahey, K. M., Hennigan, C. J., Herrmann, H., Kanakidou, M., Kelly, J. T., Ku, I.-T., McNeill, V. F., Riemer, N., Schaefer, T., Shi, G., Tilgner, A., Walker, J. T., Wang, T., Weber, R., Xing, J., Zaveri, R. A. and Zuend, A.: The Acidity of Atmospheric Particles and Clouds, Atmospheric Chem. Phys. Discuss., 1–143, doi:https://doi.org/10.5194/acp-2019-889, 2019.

Referee #2 - Eleanor Browne

Rivellini et al made ambient measurements of aerosol chemical composition with an SP-AMS on the campus of the National University of Singapore. PMF analysis was performed on the data and the authors investigated how the inclusion of rBC and metals into the PMF affected the interpretation of the PMF results. Overall, this is an interesting data set that highlights how rBC and metal measurements can enhance our understanding of aerosol sources.

Author's response: We thank for the positive comments from the reviewer. We have provided our point-to-point responses below (in blue colour) to address the questions/comments as shown below:

Major comments

1) The SP-AMS calibrations and data analysis need to be described in more detail. In particular, CE needs to be considered/discussed in more detail. Is there evidence for the morphology and coating of the rBC particles varying at all over the course of the measurements (and consequently a varying CE)? How would a varying CE affect the interpretation of the measurements and the PMF results?

Author's Response: We conducted four calibrations using ammonium nitrate and Regal black particles as described in the original manuscript. To ensure the quality of calibration, the inter-instrument comparisons have be conducted to show that our SP-AMS calibrations for both rBC and NR-PM are reasonable. The SP-AMS measurements were compared with other co-located measurements from an aethalometer (model AE33, Magee scientific), an OC/EC analyser (Sunset Laboratory) and a Monitor for AeRosols and GAses in ambient air analyzer (MARGA, Metrohm) over the sampling period.

Sulfate (SO_4^{2-}) and organic mass concentrations from the SP-AMS (CDCE-corrected) were compared to SO_4^{2-} and OM measured by the MARGA and the OC/EC analyser, respectively (Figure S3a and b in the revised SI). Aside from the good correlations that underline a good temporal response from all instruments, the slopes are in the range of 0.81-0.88, suggesting that the mass concentrations of SO_4^{2-} and organic measured by the SP-AMS are ~12-19% lower than those measured by the MARGA and the OC/EC analyser, respectively. This could be partially explained by the 1 µm cut-size of the SP-AMS, while the two other instruments were measuring $PM_{2.5}$.

The rBC mass concentrations (CE = 0.6) were compared with BC and EC measured by the aethalometer and the OC-EC analyser, respectively (Figure S3c and d in the revised SI). Scatter plots of those comparisons show Pearson coefficients > 0.84, and respective slopes of 0.83 and 1.10, supporting that CE = 0.6 for rBC is a reasonable CE correction approach. The following sentences and Figures S3 have been added to the revised manuscript and SI based on the above observations:

Page 2 lines 7-9: "Other co-located instruments for $PM_{2.5}$ characterizations include an aethalometer (AE33, Magee Scientific), a Monitor for Aerosols and Gases (MARGA, Metrohm) and a semi-continuous organic and elemental carbon (OC/EC) analyser (Sunset Laboratory)."

Page 4 lines 27-29: "The campaign averages of RIE_{rBC} and RIE_{NH4} were 0.15 (±0.04) and 4.24 (±0.04), respectively. The default RIE values of nitrate (1.1), sulfate (1.2) and organics (1.4) were used for respective mass concentration quantification (Jimenez, 2003)."

Page 4 lines 33-38: "The SP-AMS measurements were compared with the sulfate and OM concentrations measured by the MARGA and the OC/EC analyser, respectively, showing strong temporal (r = 0.77 and 0.93) and quantitative (slopes = 0.81 and 0.88) agreements between these measurements (Figure S3a and b). A collection efficiency (CE) of 0.6 was used for rBC quantification

due to incomplete overlap between the laser vaporizer and the particle beam (Willis et al., 2014). The corrected rBC concentrations were also comparable to those measured by the aethalometer (r = 0.96, slope = 0.83) and the EC measured by the OC/EC analyser (r = 0.84, slope = 1.1) (Figure S3c and d)."

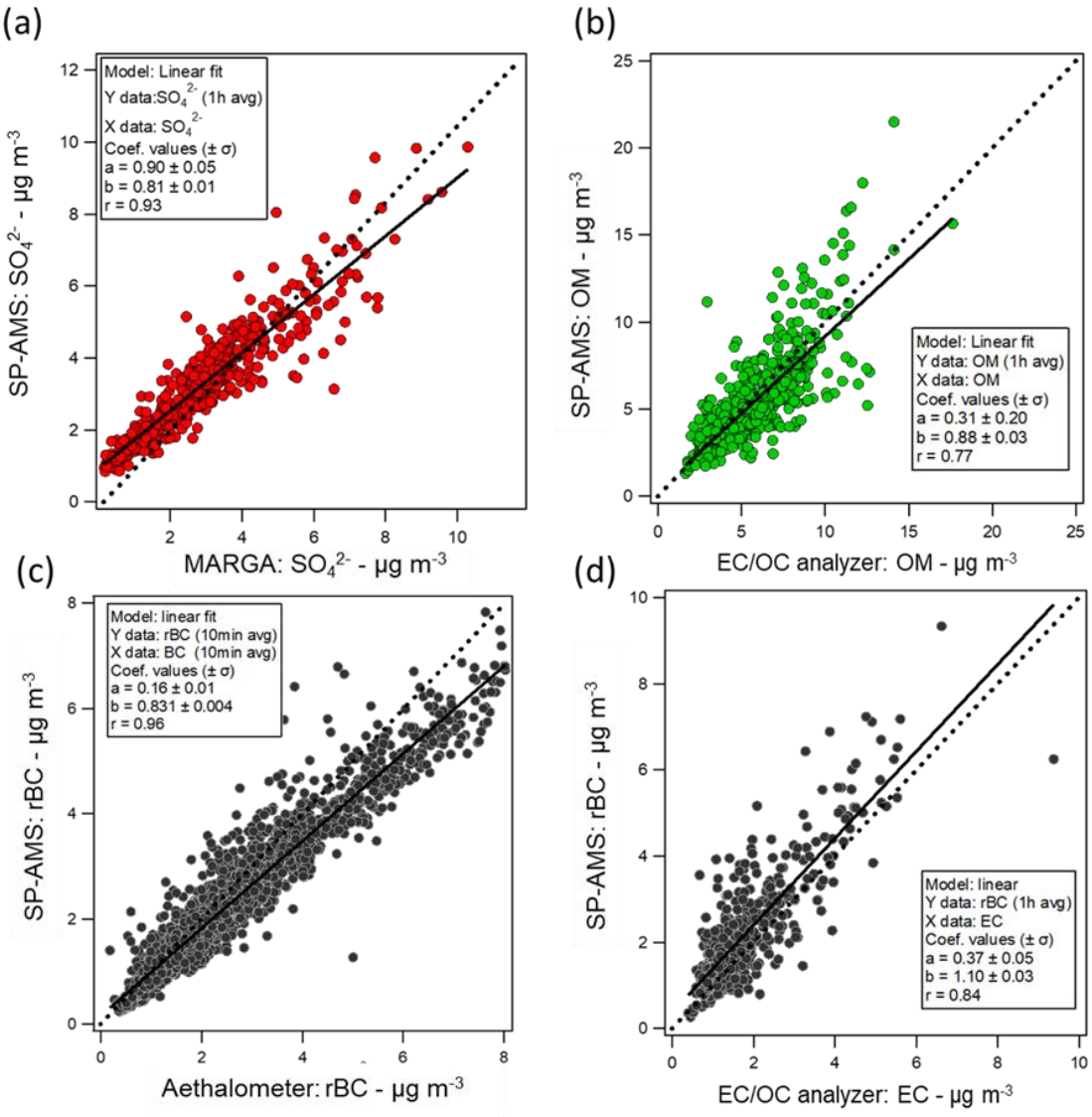

Figure S3: Scatter plots of (a) the hourly-averaged SO_4^{2-} mass concentration measured by the SP-AMS and MARGA, (b) and the hourly-averaged OA and OM (estimated from OC concentration using a 2.2 conversion factor) mass concentrations measured by the SP-AMS and OC/EC analyser, respectively. Comparisons of 10-min averaged rBC mass concentrations measured by the SP-AMS with (c) BC and (d) EC mass concentrations measured by the aethalometer and OC/EC analyser, respectively.

We agree with the reviewer that having the knowledge of coating and morphology of the BC-containing particles would be useful in determining the time-dependent CDCE of rBC measurements. However, the SP-AMS configuration used in this study (i.e., dual vaporization scheme) cannot provide further information on coating thickness and rBC morphology. Note that there is no standard approach for determining CDCE of rBC measured by the SP-AMS within the scientific community. In this work, we determined the CDCE of rBC by comparing BC (denoted as BC_{AE33} here after) and EC measured by the aethalometer and the OC/EC analyser, respectively. Comparisons between mass concentrations of our CE-corrected rBC ($rBC_{CE=0.6}$) with BC_{AE33} and EC give good Pearson coefficients of 0.96 and 0.71

and slopes of 0.83 and 1.10, respectively (Figure S3c and d). The histogram of CDCE determined for rBC using the two co-located instruments are reported in Figure S2b and c. The logarithmic distributions are centred on ~0.52 (±0.18) for aethalometer-based CDCE ($CDCE_{AE33}$) and 0.69 (±0.34) for OC/EC-based CDCE ($CDCE_{ECOC}$). These results are in a good agreement with the average CE value of 0.6 suggested by Willis et al., (2014) based on laboratory investigation.

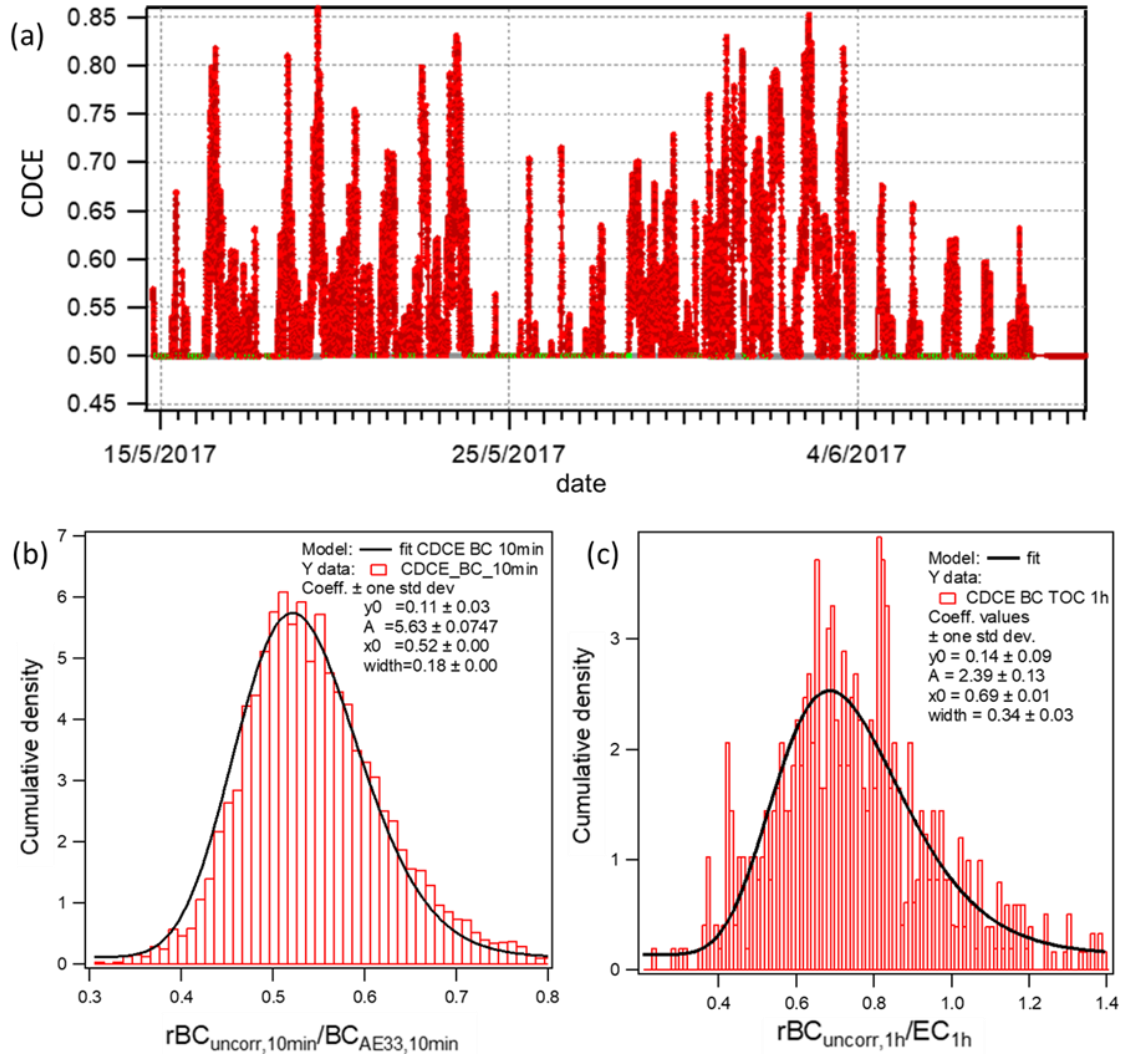

Figure S2: (a) Time series of composition-dependent collection efficiency ($CDCE_{Mid}$) determined over the entire campaign. Cumulative frequency of (b) aethalometer-based CDCE and (c) OC/EC-based CDCE, and their respective lognormal fitting determined over the entire campaign (with the fitting parameters corresponding to the following equation: $Y = y_0 + A \exp\left\{-\left[\frac{\ln(x/x_0)}{width}\right]^2\right\}$).

To evaluate the potential impact of CDCE of rBC and OA on our PMF results, three additional PMF analysis were performed by applying CDCE for rBC and/or OA, while other PMF setting remains unchanged. The metal ion signals were corrected to nitrate equivalent mass concentrations by assuming their RIE values equal to 1.

- Laser-off OA corrected by CDCE that were calculated based on the approach described by Middlebrook et al., (2012) ($CDCE_{Mid}$)

- Laser-on $CDCE_{Mid}$-corrected OA and $CDCE_{AE33}$-corrected C_n^+
- Laser-on $CDCE_{Mid}$-corrected OA and $CDCE_{AE33}$-corrected C_n^+ and metal ions

Comparisons between the CDCE-corrected results and the corresponding base cases reported in the main text (i.e., laser-off OA, laser-on OA + C_n^+ and laser-on OA + C_n^+ + metals) are shown in Table S4. Note that all PMF runs lead to five-factor solution (i.e., HOA, O-HOA, COA, LO-OOA and MO-OOA). Below is the brief summary of some major changes:

- OA fragments as PMF input: The time series of OA factors determined with $CDCE_{Mid}$ applied are similar to those without correction (i.e., Pearson coefficients > 0.91). Applying $CDCE_{Mid}$ correction result in 19-27% changes in the mass concentrations of each factor.

- OA, rBC and metals as PMF input: These modifications of PMF input do not make significant impacts on the relative contribution of each factor to the total OA and rBC. Except for the HOA factor, its contribution to the total rBC mass decreased from 44% to 33%. The C_1^+/C_3^+ ratios for MO-OOA are much more sensitive to CDCE corrections (i.e., increased from. 0.29-0.54 to 1.57-1.67) compared to other PMF factors. Even without applying CDCE correction, the C_1^+/C_3^+ ratios for MO-OOA varied between 0.29 and 0.54. Due to such large variations between cases, in addition to COA, no C_1^+/C_3^+ ratios were reported for MO-OOA in the main text.

- The CDCE corrections can affect the contributions of the five metals from each PMF factor to their total signals as shown in Table 1. The changes in the contributions of sodium and nickel from the LO-OOA and HOA factors to their total signals are relatively large compared to other metals and OA factors. It is important to emphasise that a few key observations remain unchanged: (1) K^+ and Rb^+ are strongly associated with MO-OOA, (2) V^+ is mainly associated with LO-OOA, and (3) Na^+ is associated with a few OA factors that are related to combustion emissions (i.e., LO-OOA, O-HOA, and HOA).

Overall, applying CDCE corrections for OA, rBC and metals do not result in substantial changes in our interpretations for most of the key observations. The discussion and conclusion developed based on the distribution of metals to different OA factors remains unchanged. Therefore, the original PMF results are used as a base case in our discussion in the main text. Table 1 shows the possible ranges of different parameters based on the results obtained from the CDCE-corrected PMF analysis. Table S4 summarizes the results of pre- and post-CDCE-corrected PMF analysis (Pre-CDCE: PMF solution obtained by the CDCE-corrected input matrices, Post-CDCE: PMF solution corrected by CDCE).

The above information has been added to the supplementary information. The following sentences have been added in the revised experimental section so that the readers can follow the detail of PMF analysis and results.

Page 5, lines 34-37: "The time dependent collection efficiency (or CDCE) of rBC were determined based on the BC measured by the aethalometer (Figure S2b). Additional PMF analysis, with CDCE applied on the input matrix for both OA and refractory components, were conducted (see details in Text S1 of the supplementary information). The PMF results were compared with those obtained without CDCE applied on the input matrix as shown in Table 1 and S4."

Table 1: Top: Carbon fragment ratios observed by the laser-on measurement for each PMF factor. The underlined number represents the results with both rBC fragments and trace metal ions included as PMF input. Bottom: Contribution of each PMF factor to the total signal of specific metal ions. For the entire table, the values in parenthesis are the one obtained from PMF with CDCE-corrected input matrix (see details in Text S1 and Table S4 of the supplementary information).

PMF factors	**HOA**	**O-HOA**	**COA**	**LO-OOA**	**MO-OOA**
Carbon fragments ratios					
C_1^+/C_3^+	0.66 (0.63) 0.65 (0.62)	1.00 (0.90) 1.00 (0.89)	NA*	0.81 (0.88) 0.79 (0.85)	NA#
C_2^+/C_3^+	0.38 (0.39) 0.38 (0.39)	0.41 (0.40) 0.41 (0.40)	NA*	0.39 (0.41) 0.41 (0.40)	NA#
Contribution of each factor to the total signal of specific metal ions (fraction)					
Na^+	0.35 (0.22)	0.14 (0.17)	< 0.01 (< 0.01)	0.45 (0.58)	0.06 (0.03)
K^+	0.23 (0.23)	0.19 (0.18)	< 0.01 (< 0.01)	<0.01 (0.05)	0.58 (0.54)
V^+	0.21 (0.08)	0.09 (0.16)	< 0.01 (< 0.01)	0.70 (0.76)	< 0.01 (< 0.01)
Ni^+	0.38 (0.22)	0.20 (0.22)	< 0.01 (< 0.01)	0.29 (0.45)	0.13 (0.11)
Rb^+	0.15 (0.15)	0.19 (0.19)	< 0.01 (< 0.01)	<0.01 (0.01)	0.66 (0.65)

* None of the refractory C_n^+ fragments were associated with the COA factor

Large variations of C_n^+ fragment ratios between cases, hence the ratios were not reported for MO-OOA

Table S4: Comparisons of the PMF results obtained from different CDCE correction approach (Pre-CDCE: PMF solution obtained by the CDCE-corrected input matrices, Post-CDCE: PMF solution corrected by CDCE). The post-CDCE solutions represent the corresponding base cases reported in the main text, Figure 3, and Figure S4.

PMF factors	**LO-OOA**			**MO-OOA**			**COA**			**O-HOA**			**HOA**		
Laser status	OFF	ON		OFF	ON		OFF	ON		OFF	ON		OFF	ON	
Type of PMF	OA	+ C_n^+	+ C_n^++ metal	OA	+ C_n^+	+ C_n^++ metal	OA	+ C_n^+	+ C_n^++ metal	OA	+ C_n^+	+ C_n^++ metal	OA	+ C_n^+	+ C_n^++ metal
Contribution to total OA mass (%)															
Post-CDCE	10.4	12.6	13.1	32.1	24.5	26.7	11.7	14.6	15.4	26.4	22.2	22.0	19.4	23.7	22.8
Pre-CDCE	12.4	12.3	12.1	30.8	28.5	29.6	12.6	16.3	17.8	21.0	20.6	19.7	23.2	22.2	21.4
Contribution to total rBC mass (%)															
Post-CDCE	NA	29.2	30.1	NA	6.2	6.4	NA	1.3	1.4	NA	20.1	20.7	NA	43.1	44.4
Pre-CDCE	NA	29.9	31.5	NA	7.4	8.8	NA	1.8	2.3	NA	26.5	24.4	NA	34.4	33.0
C_1^+/C_3^+															
Post-CDCE	NA	0.81	0.79	NA	0.54	0.29	NA	NA	NA	NA	1.00	1.00	NA	0.66	0.65
Pre-CDCE	NA	0.88	0.85	NA	1.76	1.57	NA	NA	NA	NA	0.90	0.89	NA	0.63	0.62
Time series - correlation coefficient (r)															
Post- vs. Pre-CDCE	0.98	0.97	0.91	0.99	0.99	0.99	0.98	0.97	0.96	0.89	0.93	0.94	0.99	0.97	0.97
Time series – slope															
Post- vs. Pre-CDCE	1.17	1.06	1.06	0.96	0.99	1.09	1.07	0.86	0.83	0.81	1.05	1.11	1.27	1.04	1.10
Normalized mass spectra - correlation coefficient (r)															
Post- vs. Pre-CDCE	1.00	0.95	0.94	1.00	1.00	0.99	1.00	0.93	0.92	1.00	0.99	0.99	0.97	0.99	0.99

2) In Sect. 3.4, the C1/C3 analysis should include a discussion about how uncertainty in the contribution of C1+ from non-refractory organic aerosol affects the interpretation of the ratio, particularly since a constant C1/C3 ratio was used to as a correction factor (Sect. 2.2). It may be beneficial to investigate the ratio of other Cx ions (e.g., C4/C3) to provide insight into the possible contribution of organics to C1.

Author's response: The C_1^+/C_3^+ ratio of 0.625 is used to calculate the total rBC mass concentrations. However, this correction was not applied when generating the PMF matrix. Instead, we applied Wang et al (2018) method to obtain the refractory fraction of C_n^+ for individual OA factor (i.e., correcting total C_n^+ fragments obtained from laser-on PMF by subtracting the organic fraction of C_n^+ ions retrieved from laser-off PMF). The lower intensities of the C_4^+-C_9^+, relatively to C_1^+-C_3^+ ions, can be strongly affected by neighbouring peaks (e.g. C_4^+ and SO^+), hence we did not report their values in the manuscript. To make this information clear, the related sentence has been revised as following.

Page 5 line 21-24: "Note that the interference of non-refractory organic signals on refractory C_n^+ fragments were subtracted based on the method described in Wang et al. (2018), and hence the C_1^+ fragment was not corrected based on the C_3^+ fragment, in the PMF analysis."

3) Sect. 3.5.1 would be strengthened by a more detailed discussion regarding urban sources of metals and including more metals in the analysis.

Author's response: Same response as reviewer #1, it is important to include all the detectable metal signals in the PMF analysis if possible. However, we only reported metals with their average values higher than the limit of detection (Table S2) determined by the particle-free air to ensure the quality of our data analysis. Nickel is a marginal case but a large fraction of its signal remain above its detection limit for investigating the V+/Ni+ ratio. To make this point clear, we have revised the sentence as shown below.

Page 5 lines 24-25: "Lastly, five metal ions (K^+, Na^+, Ni^+, V^+, Rb^+) were included into the PMF model (Figure S4g-i) as the majority of their signals were higher than their respective limit of detection (Table S2)."

Furthermore, we have followed the recommendations from reviewer #1 to include more possible sources of metals, such as biomass burning emissions for Na^+ and coal combustion emissions for Rb^+, in our discussion. Below are a few sentences/paragraphs that we have modified. Please see more detail of modification in the revised version highlighted in the point-by-point responses to reviewer #1.

Page 12 lines 5-7: "Based on the PMF results that includes trace metal ions, sodium (Na^+) was mainly associated with HOA, O-HOA and LO-OOA (Figure 5a) that could be due to different types of fossil fuel combustion emissions (e.g., local traffic, shipping, and various industrial activities) as discussed in Section 3.4."

Page 12 lines 20-23: "Biomass burning can be a possible source of Na^+ (Hsu et al., 2011) but no major fresh biomass burning emissions were observed in this study. The MO-OOA factor is suspected to be more influenced by aged regional biomass burning emissions (see more discussion in Section 3.5.2) but Na^+ was not strongly associated with this factor."

Page 13, lines 27-30: "The regional origin of K^+, Rb^+, $C_2H_4O_2^+$ and MO-OOA were investigated through their PSCF. Their PSCF graphs (Figures 6d and S15a- c) show several common origins with high probability that the highest concentrations could be influenced by biomass burning events from Indonesia (Figure S12a). Nevertheless, coal-fired power plants are located nearby the identified

hotspots of Rb^+ and K^+ (Figure S12b) so that a regional transport of coal-fired power plant emissions alongside biomass burning plumes were possible".

Additionally, the potential contribution of oceanic sources to Na^+ should be discussed in more detail. While the authors state that Na+ and Cl- exhibit poor temporal correlation, I assume this is for the whole data set. If one filters by wind direction (and thus sea breeze) does this still hold? Additionally, is there an interpretation for the large contribution of Na+ in LO-OOA? Finally, does the fact that different C1/C3 ratios were seen for LO-OOA and HOA (the factors with the strongest Na+ contribution) tell us anything about the different sources of Na+?

Author's response: Thanks for the suggestion on the data analysis. Firstly, the comparison between Na^+ and Cl^- under sea breeze conditions do not improve the correlation, with $r < 0.1$ (n=3384). The large contribution of Na^+ in LO-OOA can be due to the fact that this OA factor is associated with industrial emissions. In particular, LO-OOA had the second largest contribution to the total rBC, suggesting that at least a fraction of rBC from industrial emissions could act as effective condensation sinks of LO-OOA produced via the photochemistry along their dispersion as discussed in Section 3.4 of the original manuscript. Finally, the different C_1^+/C_3^+ ratios between LO-OOA and HOA can provide insight to the possible sources of Na^+ as discussed in Sections 3.4 and 3.51. To better connect the two Sections, a sentence has been added in Section 3.5.1, and the paragraph in Section 3.4 has been revised as following.

Section 3.5.1, page 12, lines 5-7: "Based on the PMF results that includes trace metal ions, sodium (Na^+) was mainly associated with HOA, O-HOA and LO-OOA that could be due to different types of fossil fuel combustion emissions (e.g., local traffic, shipping, and various industrial activities) as discussed in Section 3.4."

Section 3.5.1, page 12, Lines 18-20: "However, it is important to emphasize that Na^+ and Cl^- exhibit rather poor temporal correlations ($r < 0.30$) for both laser-off and laser-on data regardless the influences of sea breeze."

Section 3.4, page 11, lines 13-27: "The C_1^+/C_3^+ ratios of rBC associated with HOA was 0.66 (±0.07) , which was within the range of those emitted from aircraft-turbine, regal black (i.e., a BC standard for SP-AMS calibration) and particles produced by a propane diffusion flame (0.50 – 0.78) and, more importantly, close to those reported for diesel engine exhaust (Carbone et al., 2019; Corbin et al., 2014; Onasch et al., 2012). Furthermore, the size distribution of unit mass resolution data shows lower *m/z* 12-to-*m/z* 36 ratios (a proxy for C_1^+/C_3^+) for particles with d_{va} smaller than 100 nm (Figure S11a). This suggests that rBC particles with relatively small diameter were mainly associated with fresh traffic emissions (Massoli et al., 2012). Our results illustrate that rBC transported from industrial area and shipping ports gave C_1^+/C_3^+ ratios closer to unity (i.e., LO-OOA = 0.79 (±0.10) and O-HOA = 1.00 (±0.11), which is similar to the previous observations for soot particles emitted from a marine engine using heavy-fuel-oil (Corbin et al., 2018), rBC-containing particles emitted from chemical and petrochemical industries (Wang et al., 2018), and rBC with high fullerene content (Canagaratna et al., 2015a; Corbin et al., 2014). The NWR and diurnal plots of C_1^+/C_3^+ ratio (Figure 4c and d) clearly show that rBC with higher C_1^+/C_3^+ ratios were transported to the site by sea breeze from the southwest direction, which are consistent with our PMF results that O-HOA and LO-OOA were influenced by industrial emissions and were associated with rBC with higher C_1^+/C_3^+ ratios compared to other OA components."

4) To me, it seems that the last sentence of the introduction and the last paragraph of the conclusions overstate the implications and applications of the manuscript. Optical properties of aerosols were not

discussed in the manuscript, so the inclusion in the introduction and conclusion seems out of place. Moreover, the work of Kasthuriarachchi et al (2019) is under review so the inclusion here is somewhat misleading. I suggest that the authors consider revising this paragraph and the last sentence of the introduction to better reflect the material covered in this study.

Author's response: The last sentence of the introduction has been removed as suggested. In addition, the last paragraph of conclusion has been revised as following. In particular, the observations from Kasthuriarachchi et al (2020) has been removed from the conclusion.

Page 14, lines 37-38 to Page 15, lines 1-9: "More broadly, the improved source identification for OA and rBC can provide useful information to further investigate the effects of atmospheric aging on their physio-chemical properties. For example, this work highlights the potential influences of regional biomass burning and coal combustion emissions to MO-OOA component, which may provide important insight into how light absorbing properties of OA (i.e., brown carbon) evolve with transport and aging. Recently, Dasari et al. (2019) provided field evidence for the bleaching of brown carbon during their transport by photo-oxidation and that photo-dissociation can occur in the South Asian outflow based on measurements near and away from specific combustion sources, including biomass burning and traffic. Furthermore, this type of PMF analysis could be applied to analyze the sources and characteristics of rBC-containing particles exclusively (i.e., rBC core with organic coatings) in order to advance our understanding on the effects of primary emissions and/or atmospheric processing on BC light absorption enhancement caused by the lensing effect."

Minor comments

-It would be helpful to explicitly pinpoint some of the main industrial sources (such as the oil refinery discussed in the introduction and shipping ports) in Figure S1a.

Authors' response: The major industrial activities occurring on Jurong Island (i.e., an industrial zone located at the southwest direction of sampling site) have been added in Table S1. Additional pins have been added to illustrate their locations in Figure S1a.

-Page 7 lines 12-15: Regarding the production of organo-sulfur compounds in acidic sulfate plumes – this seems rather poorly supported at the moment. As it does not advance the main focus of the paper, I suggest removing. -Figure S4a the legend (colours based on CH2SO) does not match the caption (data originating from SW and other directions).

Authors' response: We agree with the reviewer and have removed the sentence regarding the production of organo-sulfur compounds in acidic sulfate plumes. The caption has been corrected to match the figure (Figure S6 in the revised version).

-Figure S4d needs a color scale. The 2 modes (discussed at the end of page 6) are also not apparent from this figure, perhaps due to the color scale used. Currently it looks to me more like the distribution broadens when the concentration increases in the middle of the day.

Authors' response: The colour scale has been added to Figure S6a (former Figure S4d). We agree with the reviewer that the distribution of sulfate particles broaden in the middle of the day. It is worth noting that the Figure S6a is the average of the entire campaign. If we separate the strong sulfate plumes from

the entire dataset, Figure S6d (former Figure S4b) shows that the sulfate particles size is smaller for the strong sulfate plumes compared to the rest of periods. The sentences have been revised as following.

Page 7, lines 21-26: "This particle acidity dependence seems to coincide with diurnal variations of SO_4^{2-} size distribution. Throughout the day, relatively large sulfate particles are observed with their vacuum aerodynamic diameter (d_{va}) peaked at ~400 nm, whereas those encountered during the sea breeze present a broader mode with d_{va} ranging between 200 and 400 nm (Figure S6a and d). This suggests that a large fraction of acidic SO_4^{2-} particles observed during the sea breeze period were freshly formed in the atmosphere."

-Discuss figures in order (e.g., Fig. S6 is currently referenced before S5). Cite panels of figures in order (for instance, the panels of Fig. S4 are cited out of order).

Authors' response: Both manuscript and SI figures have been re-arranged accordingly.

-Figure S5: The wording in the caption is unclear, specifically "... both filtered from 25th to 28th of May, over the campaign." Is "both" just COA and HOA? Does it mean that only the 25th to 28th was included?

Authors' response: We agree with the reviewer and have reworded the caption as follow:

Figure S8 (former Figure S5): "Figure S8: Diurnal cycles of (a) N:C (laser-off mode), (b) NO_x, (c) CO, (d) COA, (e) HOA, and (f) O_3 over the campaign. The plain and dotted lines represent the medians and averages values, respectively. The shaded regions represent the 25th and 75th percentiles. Note that data between May 25th to 28th were excluded for HOA and COA due to the strong unknown emission during the nighttime."

-In Sect 3.5.2, why use m/z 60 rather than the HR ion (C2H4O2+)?

Authors' response: The f_{60} was calculated using organic fragment signals at $C_2H_4O_2^+$. We have replaced f_{60} and m/z 60 by $f_{C2H4O2+}$ and m/z $C_2H_4O_2^+$, respectively, in Section 3.5.2 and corresponding figures.

-Page 10 line 27: rather than "inferior" use "smaller than"

Authors' response: The correction has been made.

-Page 12 line 23: I do not find the similar size distributions for m/z 39 and 60 to be convincing evidence for a BBOA source. m/z 60 is the only individual organic ion shown in Fig. S8b. How unique is the size distribution for m/z 60 compared to other individual organic ions?

Authors' response: We agree with the reviewer so that the sentence has been removed. However, we have decided to keep the Figure in SI as literature information.

-Page 12 line 19: should this be Figure 5d rather than 3c and 4b?

Authors' response: We thank the reviewer for pointing out this error. It has been corrected in the revised version.

References:

Canagaratna, M. R., Massoli, P., Browne, E. C., Franklin, J. P., Wilson, K. R., Onasch, T. B., Kirchstetter, T. W., Fortner, E. C., Kolb, C. E., Jayne, J. T., Kroll, J. H. and Worsnop, D. R.: Chemical Compositions of Black Carbon Particle Cores and Coatings via Soot Particle Aerosol Mass Spectrometry with Photoionization and Electron Ionization, J. Phys. Chem. A, 119(19), 4589–4599, doi:10.1021/jp510711u, 2015.

Carbone, S., Timonen, H. J., Rostedt, A., Happonen, M., Rönkkö, T., Keskinen, J., Ristimaki, J., Korpi, H., Artaxo, P., Canagaratna, M., Worsnop, D., Canonaco, F., Prévôt, A. S. H., Hillamo, R. and Saarikoski, S.: Distinguishing fuel and lubricating oil combustion products in diesel engine exhaust particles, Aerosol Sci. Technol., 0(0), 1–14, doi:10.1080/02786826.2019.1584389, 2019.

Corbin, J. C., Sierau, B., Gysel, M., Laborde, M., Keller, A., Kim, J., Petzold, A., Onasch, T. B., Lohmann, U. and Mensah, A. A.: Mass spectrometry of refractory black carbon particles from six sources: carbon-cluster and oxygenated ions, Atmos Chem Phys, 14(5), 2591–2603, doi:10.5194/acp-14-2591-2014, 2014.

Corbin, J. C., Mensah, A. A., Pieber, S. M., Orasche, J., Michalke, B., Zanatta, M., Czech, H., Massabò, D., Buatier de Mongeot, F., Mennucci, C., El Haddad, I., Kumar, N. K., Stengel, B., Huang, Y., Zimmermann, R., Prévôt, A. S. H. and Gysel, M.: Trace Metals in Soot and PM $_{2.5}$ from Heavy-Fuel-Oil Combustion in a Marine Engine, Environ. Sci. Technol., 52(11), 6714–6722, doi:10.1021/acs.est.8b01764, 2018.

Dasari, S., Andersson, A., Bikkina, S., Holmstrand, H., Budhavant, K., Satheesh, S., Asmi, E., Kesti, J., Backman, J., Salam, A., Bisht, D. S., Tiwari, S., Hameed, Z. and Gustafsson, Ö.: Photochemical degradation affects the light absorption of water-soluble brown carbon in the South Asian outflow, Sci. Adv., 5(1), eaau8066, doi:10.1126/sciadv.aau8066, 2019.

Hsu, L.-J., Alwahabi, Z. T., Nathan, G. J., Li, Y., Li, Z. S. and Aldén, M.: Sodium and Potassium Released from Burning Particles of Brown Coal and Pine Wood in a Laminar Premixed Methane Flame Using Quantitative Laser-Induced Breakdown Spectroscopy:, Appl. Spectrosc., doi:10.1366/10-06108, 2011.

Jimenez, J. L.: Ambient aerosol sampling using the Aerodyne Aerosol Mass Spectrometer, J. Geophys. Res., 108(D7), doi:10.1029/2001JD001213, 2003.

Massoli, P., Fortner, E. C., Canagaratna, M. R., Williams, L. R., Zhang, Q., Sun, Y., Schwab, J. J., Trimborn, A., Onasch, T. B., Demerjian, K. L., Kolb, C. E., Worsnop, D. R. and Jayne, J. T.: Pollution Gradients and Chemical Characterization of Particulate Matter from Vehicular Traffic near Major Roadways: Results from the 2009 Queens College Air Quality Study in NYC, Aerosol Sci. Technol., 46(11), 1201–1218, doi:10.1080/02786826.2012.701784, 2012.

Middlebrook, A. M., Bahreini, R., Jimenez, J. L. and Canagaratna, M. R.: Evaluation of Composition-Dependent Collection Efficiencies for the Aerodyne Aerosol Mass Spectrometer using Field Data, Aerosol Sci. Technol., 46(3), 258–271, doi:10.1080/02786826.2011.620041, 2012.

Onasch, T. B., Trimborn, A., Fortner, E. C., Jayne, J. T., Kok, G. L., Williams, L. R., Davidovits, P. and Worsnop, D. R.: Soot Particle Aerosol Mass Spectrometer: Development, Validation, and Initial Application, Aerosol Sci. Technol., 46(7), 804–817, doi:10.1080/02786826.2012.663948, 2012.

Wang, J., Wu, Y., Ge, X., Shen, Y., Ge, S. and Chen, M.: Characteristics and sources of ambient refractory black carbon aerosols: Insights from soot particle aerosol mass spectrometer, Atmos. Environ., 185, 147–152, doi:10.1016/j.atmosenv.2018.05.011, 2018.

Willis, M. D., Lee, A. K. Y., Onasch, T. B., Fortner, E. C., Williams, L. R., Lambe, A. T., Worsnop, D. R. and Abbatt, J. P. D.: Collection efficiency of the soot-particle aerosol mass spectrometer (SP-AMS) for internally mixed particulate black carbon, Atmos Meas Tech, 7(12), 4507–4516, doi:10.5194/amt-7-4507-2014, 2014.

Characterization of carbonaceous aerosols in Singapore: insight from black carbon fragments and trace metal ions detected by a soot-particle aerosol mass spectrometer

Laura-Hélèna Rivellini[1], Max G. Adam[2#], Nethmi Kasthuriarachchi[2], Alex K.Y. Lee[1,2]

[1] NUS Environmental Research Institute, National University of Singapore, 117411, Singapore
[2] Department of Civil and Environmental Engineering, National University of Singapore, 117576, Singapore
[#] Now at Department of Civil and Environmental Engineering, National University of Singapore, 117576, Singapore

Correspondence to: Alex K. Y. Lee (ceelkya@nus.edu.sg)

Abstract. Understanding sources and atmospheric processes that can influence the physio-chemical properties of carbonaceous aerosols are essential to evaluate their impacts on air quality and climate. However, resolving the sources, emission characteristics and aging processes of carbonaceous aerosols in complex urban environments remain challenging. In this work, a soot-particle aerosol mass spectrometer (SP-AMS) was deployed to characterize organic aerosols (OA), refractory BC (rBC) and trace metals in Singapore, a highly urbanized city with multiple local and regional air pollution sources in the tropical region. rBC (C_1^+–C_9^+) fragments and trace metals ions (K^+, Na^+, Ni^+, V^+ and Rb^+) were integrated into our positive matrix factorization of OA. Two types of fossil fuel combustion-related OA with different degree of oxygenation were identified. This work provides evidence that over 90% of rBC was originated from local combustion sources with a major part related to traffic and ~30% of them associated with fresh secondary organic aerosol (SOA) produced under the influences of shipping and industrial emissions activities (e.g., refineries and petrochemical plants) during daytime. The results also show that ~43% of the total rBC was emitted from local traffic, and the rest of rBC fraction due to multiple sources, including vehicular, shipping and industrial emissions, being not fully resolved. There was only a weak association between the cooking-related OA component and rBC. Although there was no observable biomass burning episode during the sampling period, K^+ and Rb^+ were mainly associated with the more-oxidized oxygenated OA component, indicating potential contributions of regional biomass burning and/or coal combustion emissions to this aged OA component. Furthermore, the aerosol pollutants transported from the industrial area and shipping ports gave higher C_1^+/C_3^+ and V^+/Ni^+ ratios than those associated with traffic. The observed association between Na^+ and rBC suggests that the contribution of anthropogenic emissions to total particulate sodium should not be ignored in coastal urban environments. Overall, this work demonstrates that rBC fragments and trace metal ions can improve our understanding on the sources, emissions characteristics and aging history of carbonaceous aerosol (OA and rBC) in this type of complex urban environments.

1. Introduction

Rapid economic growth of Southeast Asia have resulted in frequent air pollution episodes in the region, primarily due to emissions from different types of fuel and biomass combustions (UN Environment, 2014). Besides typical urban emissions (e.g., local traffic), Singapore is a highly urbanized and densely populated city located at the south end of the Malaysian Peninsula that can be seasonally impacted by air pollutants, especially fine particulate matter, caused by agricultural burning and wildfire events from the neighboring countries (Atwood et al., 2013; Salinas et al., 2013). Singapore is the major maritime hub in Southeast Asia. According to the World Shipping Council, Singapore has the world's second-busiest port in terms of shipping tonnage (World Shipping Council, 2019). Deep-sea cargo ships typically burn heavy residual oil and hence the impacts of ship emissions on both local and regional particulate pollution can be substantial (Saputra et al., 2013; Velasco and Roth, 2012). Furthermore, one of the world's largest oil refinery and manufacturing complexes is located in the industrial zone of Singapore (Chou et al., 2019; Diez et al., 2019) but its potential influences on local and regional air quality remains poorly understood.

Most of the air quality studies focused on particulate pollution in Singapore have been relying on off-line chemical speciation of aerosol filter samples (Balasubramanian and Qian, 2004; Atwood et al., 2013; Yang et al., 2013; Engling et al., 2014). Although this approach can provide valuable information for characterizing sources and transports of atmospheric aerosols, higher time-resolution measurements are essential for evaluating potential impacts of short-term pollution events on air quality and tracking rapid variations of aerosol compositions due to emissions and atmospheric dynamics. In particular, a combination of real-time aerosol mass spectrometry technique and positive matrix factorization (PMF) analysis has been widely used for characterizing chemical compositions and potential sources of atmospheric submicron organic aerosols (OA) worldwide (Zhang et al., 2007b; Jimenez et al., 2009). Recently, Budisulistiorini et al. (2018) observed a strong haze event that lasted for only a few hours in Singapore due to the regional transports of air mass influenced by the wildfires in Kalimantan and Sumatra, Indonesia, in 2015 using an online aerosol chemical speciation monitor (ACSM). Two OA components caused by peat and biomass burning events, accounting for ~30% of total OA mass, could be identified based on their PMF analysis.

Combustion processes are known sources of urban carbonaceous aerosol, consisting of OA and black carbon (BC). The diversity of anthropogenic activities in Singapore can lead to complex mixtures of OA and BC with their sources being difficult to be interpreted based on the PMF analysis of OA fragments measured by on-line aerosol mass spectrometry alone. For example, although Budisulistiorini et al. (2018) could identify a primary OA (POA) component originated from local fossil fuel combustion and a secondary OA (SOA) component produced through a few possible formation mechanisms in Singapore during the haze period in 2015, only limited information on their emission characteristics and formation/aging processes could be provided. Taking the advantage of soot-particle aerosol mass spectrometer (SP-AMS) that can detect refractory BC (rBC, an operational defined term) and trace metals in addition to the non-refractory particulate matter (NR-PM, including OA, sulfate, nitrate, ammonium and chloride) (Carbone et al., 2015; Onasch et al., 2012), the primary goal of this work is to improve our understanding on the emissions characteristics and aging processes of carbonaceous aerosols in Singapore by performing three versions of PMF analysis with different model inputs obtained from our SP-AMS measurements: 1) OA fragments, 2) OA and rBC fragments (C_n^+), and 3) OA and rBC fragments and trace metal

ions. This is the first time to deploy a SP-AMS in Singapore and Southeast Asia for this type of field investigation. The results provide insights into how OA components are co-emitted and interact with BC and metal species in the atmosphere ~~and the optical properties of brown carbon, a fraction of light absorbing OA, as reported in Kasthuriarachchi et al. (2019)~~.

2. Methodology

2.1 Sampling site and co-located measurements

A SP-AMS was deployed to measure the chemical composition of atmospheric submicron aerosols (see details in Section 2.2). Other co-located instruments for $PM_{2.5}$ characterizations include an aethalometer (AE33, Magee Scientific), a Monitor for Aerosols and Gases (MARGA, Metrohm) and a semi-continuous organic and elemental carbon (OC/EC) analyser (Sunset Laboratory). Gas-phase species, including nitrogen oxides (NO_X, Horiba APNA-370), carbon monoxide (CO, Horiba APMA-370), and ozone (O_3, 2B Technologies Inc., Model 202), were also measured. The measurements were carried out from 14 May to 9 June 2017 at the E2 building (1°18'N, 103°46', 67 m above sea level) within the campus of the National University of Singapore. The measurement site is located at the southern part of Singapore, which is ~1 km away from the large-scale shipping port facilities (Figure S1a). The air quality at the site can be influenced by nearby traffic and emissions from an industrial area located at the southwest of the measurement site (Table S1).

Co-located meteorological measurements of wind speed and direction (RM Young model wind sentry set 03001), relative humidity (RH) and temperature (Vaisala model CS500), solar radiation (LI-COR model LI-200X), and rainfall (hydrological services CS700) were conducted throughout the entire sampling period. In general, the month of May falls into the inter-monsoonal period (i.e., March-May) characterized by low wind speed, whereas June to September are classified as the southwest monsoon period characterized by low rainfall levels compared to the rest of the year (NEA, 2018). During this field study, the shift from low intensity and variable winds toward stronger wind blowing from southwest was observed during the second half of May. Furthermore, the beginning of June clearly appeared under low level winds from southwest (Figure 1 and S1b). These observations suggest that the sampling period covered the transition period from late inter-monsoon to the early southwest monsoon season.

2.2. Data collection

2.2.1 Soot-particle aerosol mass spectrometer (SP-AMS)

A Teflon-coated cyclone (URG, model 2000-30ED) with a cut-off diameter of 2.5 µm was installed in the sampling inlet of the SP-AMS. The detail description of SP-AMS has been reported by Onasch et al. (2012), and thus only a brief description of its working principle is given in this section. SP-AMS is based on the design of high-resolution time-of-flight aerosol mass spectrometer (HR-ToF-MS, DeCarlo et al., 2006). HR-ToF-AMS can quantify NR-PM by flash vaporization of aerosol particles at 600ºC on a resistively heated tungsten surface. SP-AMS has an additional Nd-YAG intra-cavity infrared (IR) laser module at the wavelength of 1064nm. rBC is strongly absorbing in this wavelength, hence heating up to ~ 4000ºC for rBC vaporization (Onasch et al., 2012).

The term rBC is an operationally defined term that applies to BC particles detected by SP-AMS. The resulting gas-phase molecules are ionized by electron impact (EI) ionization method at 70 eV and analyzed by a ToF-MS. Non-refractory and refractory species that are internally mixed with soot particles, such as organics, inorganics, or trace elements, can be detected through laser vaporizer measurements (Carbone et al., 2015; Corbin et al., 2018; Onasch et al., 2012). In the present study, the SP-AMS was operated at 1 min alternating intervals between IR laser-on (i.e., dual vaporizers) and laser-off mode (i.e., tungsten vaporizer only), with a mass spectral resolving power of approximately 2000 at *m/z* 28. The vacuum aerodynamic diameter (d_{va}) of ambient particles is determined by the measured particle time-of-flight (PToF) from the chopper wheel to the tungsten vaporizer (Jayne et al., 2000).

2.2.2 Calibrations

Calibrations of the SP-AMS for quantifying NR-PM in the laser-off mode were performed by generating dried monodispersed (300nm) ammonium nitrate (NH_4NO_3) particles. The NH_4NO_3 solution was atomized by a constant output atomizer (TSI, model 3076). The aqueous droplets were subsequently dried by passing through a diffusion dryer and were size-selected using a differential mobility analyzer (DMA, TSI Inc., Model 3081). The ionization efficiency (IE_{NO3}) and the mass-based ionization efficiency ($mIENO_3$) were determined based on three sets of calibration data throughout the sampling period. Similarly, dried mono-dispersed (300nm) black carbon particles generated by atomizing the standard Regal Black (Regal 400R Pigment Black, Cabot Corp., recommended by Onasch et al., 2012) were used to determine the mass-based ionization efficiency of rBC (mIE_{rBC}) and its ionization efficiency relative to nitrate ($RIE_{rBC} = mIE_{rBC}/mIE_{NO3}$) for the quantification of rBC in the laser-on mode.

The calibration and field data were processed using the IGOR-based AMS data analysis software SQUIRREL v. 1.16I for unit mass resolution (UMR) data and PIKA, v. 1.57I for high resolution peak fitting (Sueper, 2015) with the corrected air fragment column of the standard fragmentation table based on particle-free ambient air data (Allan et al., 2004; DeCarlo et al., 2006). The sum of carbon ion clusters C_1^+-C_9^+ measured in the laser-on mode was used for quantifying rBC mass in both calibration and ambient data. The average C_1^+/C_3^+ ratio (0.65) obtained from Regal Black was used to correct the non-refractory organic interference in C_1^+ for quantification of total rBC mass loadings. The campaign averages of RIE_{rBC} and RIE_{NH4} were 0.15 (±0.04) and 4.24 (±0.04), respectively. The default RIE values of nitrate (1.1), sulfate (1.2) and organics (1.4) were used for respective mass concentration quantification (Jimenez, 2003). NR-PM were quantified based on the laser-off mode measurements and their CE were determined using the composition-dependent approach (CDCE, Figure S2a) (Middlebrook et al., 2012). Note that the sample stream was dried to less than 30% RH by a Nafion dryer (PD-200T-12 MPS, Perma Pure) throughout the sampling period in order to reduce CE uncertainties due to particle bouncing on the surface of tungsten vaporizer. The SP-AMS measurements were compared with the sulfate and OM concentrations measured by the MARGA and the OC/EC analyser, respectively, showing strong temporal (r = 0.77 and 0.93) and quantitative (slopes = 0.81 and 0.88) agreements between these measurements (Figure S3a and b). A collection efficiency (CE) of 0.6 was used for rBC quantification due to incomplete overlap between the laser vaporizer and the particle beam (Willis et al., 2014). The corrected rBC concentrations were also comparable to those measured

by the aethalometer (r = 0.96, slope = 0.83) and the EC measured by the OC/EC analyser (r = 0.84, slope = 1.1) (Figure S3c and d). Potassium (K^+), sodium (Na^+), vanadium (V^+), nickel (Ni^+) and rubidium (Rb^+) ions were detected (Table S2). The signals of these trace metal ions were not calibrated and thus their raw signals were used for investigating their temporal variations.

2.3 Data analysis

2.3.1 Positive matrix factorization of OA, rBC and metals

Positive matrix factorization (PMF) is widely used for identifying sources of OA measured by different versions of aerosol mass spectrometers (Ulbrich et al., 2009; Zhang et al., 2011). Each factor contains signals at *m/z* values, which have common source characteristics and chemical properties that can be used to trace the origin and processing history of that factor. The PMF evaluation tool (PET, v3.00D) (Ulbrich et al., 2009) was used to identify the potential sources and characteristics of OA based on the organic fragments measured in the laser-off mode. In the process of applying PMF, the ions with a signal-to-noise ratio (SNR) of $0.2 < SNR < 2.0$ were downweighted by a factor of 2. CO_2^+ related ions (O^+, HO^+, H_2O^+, CO^+) were downweighted and bad ions ($SNR < 0.2$) were removed from the analysis. The results were obtained for 8 up to 10 factors with f-peak varying from -1 to 1 and increasing in step size of 0.2. Elemental ratios (O:C, H:C and N:C) of each factor were determined using the improved-ambient method as described by Canagaratna et al. (2015b). A five-factor solution was selected as final result from OA laser-off PMF analysis.

PMF analysis was further applied to determine how rBC associate with different OA factors. For this purpose, the PMF inputs were generated using 1) organic fragments measured by the laser-on mode (Figure S4a-c) and 2) both organic and C_n^+ fragments measured by the laser-on mode (Figure S4d-f). The C_n^+ in the mass spectra of each PMF factor were used to quantify the fraction of rBC associated with the identified OA components. Note that the interference of non-refractory organic signals on refractory C_n^+ fragments were subtracted based on the method described in Wang et al. (2018), and hence the C_1^+ fragment was not corrected based on the C_3^+ fragment, in the PMF analysis. Lastly, five metal ions (K^+, Na^+, Ni^+, V^+, Rb^+) were included into the PMF model (Figure S4g-i) as the majority of their signals were higher than their respective limit of detection (Table S2). The metal ion signals were corrected to nitrate equivalent mass concentrations by assuming their RIE values equal to 1 and the K^+ signals were downweight by a factor 2. A similar approach was applied by Carbone et al. (2019) including rBC fragments, calcium ($^{42}Ca^+$) and zinc ($^{68}Zn^+$) isotopic ions, to distinguish between lubricating oil and fuel OA types emitted at the exhaust of diesel engines. Note that the correction approach for obtaining refractory C_n^+ signals can only be applied when both mass spectra and time series of each OA component identified in the laser-off and laser-on PMF analysis are similar. The scatter plots (Figure S5) and correlation coefficients (r) (Table S3) highlight the consistency of the mass spectra ($0.91 < r < 0.99$), as well as time series ($0.78 < r < 0.98$), of the five OA types identified in this work. The time dependent collection efficiency (or CDCE) of rBC were determined based on the BC measured by the aethalometer (Figure S2b). Additional PMF analysis, with CDCE applied on the input matrix for both OA and refractory components, were conducted (see details in Text S1 of the supplementary information). The PMF results were compared with those obtained without CDCE applied on the input matrix as shown in Table 1 and S4.

2.3.2 Air mass back-trajectories and wind analysis

The origins of air masses were investigated through 5 days back trajectories generated every hour (648 back trajectories in total) at the height of 64 m using the Hybrid Single-Particle Lagrangian Integrated Trajectory (HYSPLIT) model coupled with meteorological data from the Global Data Assimilation System (GDAS, 1°). This model was developed by the National Oceanic and Atmospheric Administration (NOAA) (Draxler and Rolph, 2003). A cluster analysis was performed on all the hourly back trajectories and the three identified clusters are shown in Figure S1c. The detail of the back-trajectories clustering can be find in Baker (2010) and Borge et al. (2007).

The potential sources of pollutants were investigated by using ZeFir non-parametric wind regression (NWR) and potential source contribution function (PSCF) package developed by Petit et al., (2017) under Igor Pro. These analytical methods require high time-resolution atmospheric measurements as inputs and combine them with local wind measurements for NWR and air mass back-trajectories for PSCF. The NWR is commonly employed to identify nearby sources by coupling atmospheric species concentrations with co-located wind speed and direction (Henry et al., 2009). This method consists of weighting average concentrations with each wind speed and direction couples and using two kernel smoothing functions. In this study, the NWR graphs were generated for an angle resolution of 1° and a radial resolution of 0.1 m s^{-1} and their respective smoothing parameters (or kernel parameters) have been empirically set at 5 and 2.5. For regional sources investigation, the PSCF has been favored as larger geographical scales can be studied (Polissar et al., 2001). The PSCF principle consists of redistributing high pollutant concentrations based on air mass trajectories residence time. Thus, individual species concentrations are redistributed along the trajectories into geographical emission parcels. In our study, PSCF calculation were performed considering only pollutant concentrations above their respective 75th percentile (graphic parameters: cell size = 0.1°, smoothing = 2).

3 Results and discussion

3.1 Overview of SP-AMS measurements

Figure 1a presents the time series of particle- and gas-phase species, PMF factors and meteorological parameters (i.e., solar radiation, temperature, RH, precipitation, wind direction and wind speed) measured during this field campaign. The mean concentration of total PM (i.e., NR-PM + rBC measured by the SP-AMS) observed in this campaign was 11.9 (± 5.0) µg m^{-3}, which is about one-fifth of the average concentration of 49.8 µg m^{-3} during the haze event due to the Indonesian wildfires in 2015 (Budisulistiorini et al., 2018). The main contributors to the submicronic aerosol mass loadings were OA (5.59 ± 2.66 µg m^3; 46.6%), followed by sulfate (SO_4^{2-}, 3.29 ± 1.83 µg m^3, 27.4%) and rBC (1.79 ± 0.37 µg m^3; 17.6%), whereas ammonium (NH_4^+, 0.85 ± 0.37 µg m^3; 7.1%), nitrate (NO_3^-, 0.11 ± 0.09 µg m^3; 0.9%) and chloride (Cl^-, 0.05 ± 0.04 µg m^3; 0.4%) were minor contributors (Figure 1b). The overall chemical compositions were not sensitive to the three major types of air mass back trajectories identified within the sampling period (Figure S1d).

The average RH was ~75% for temperature ranging from 26 to 32°C. The time series of wind speed and direction show a regular pattern with stronger wind speed from the southwest direction and drier condition between 13:00 and 16:00 local time (LT) (Figure S1b). This is primarily due to sea breeze phenomena that are commonly observed in Singapore during inter-monsoon period. Note that a large industrial zone is located at the southwest of the measurement site (Figure S1a). Sea breeze might carry polluted air from industry, such as oil refinery and shipping emissions, to the measurement site and the surrounding area. In particular, rBC is considered as a primary and persistent air pollutant emitted from combustion processes. While the rBC hotspot observed under low wind speed conditions was likely due to local traffic emissions, the elevated levels of rBC in the southwest sector (Figure 2) highlight the potential influences of industrial emissions of both primary and secondary pollutants on the air quality of the sampling region as discussed in Section 3.2 and 3.3. The detail of rBC sources and characteristics are discussed in Section 3.4 and 3.5.

3.2 Acidic sulfate and organo-sulfur formation during sea breeze period

The diurnal cycle of SO_4^{2-} shows a sharp increase starting from ~10:00 LT. reaching a maximum at ~15:00 LT (Figure 1c), which can be explained by the active photochemistry during daytime. The average value of 0.71 for the measured to predicted NH_4^+ ratio ($NH_4^+{}_{,meas}/NH_4^+{}_{,pred}$) (Zhang et al., 2007a) and the absence of diurnal pattern for NH_4^+ (Figure 1c) implies that gaseous ammonia were insufficient to neutralize acidic sulfate plumes within a timescale of a few hours (Attwood et al., 2014; Guo et al., 2015; Kim et al., 2015). Note that NO_3^- and Cl^- mass concentrations were too low to have substantial influences on the NH_4^+ levels. The diurnal cycle and NWR plot of $NH_4^+{}_{,meas}/NH_4^+{}_{,pred}$ ratios (Figure S6a and b) illustrate that the sulfate plumes observed during the sea breeze from southwest were more acidic than the background sulfate aerosol (Figure S6c). This particle acidity dependence seems to coincide with diurnal variations of SO_4^{2-} size distribution. Throughout the day, relatively large sulfate particles are observed with their vacuum aerodynamic diameter (d_{va}) peaked at ~400 nm, whereas those encountered during the sea breeze present a broader mode with d_{va} ranging between 200 and 400 nm (Figure S6a and d). This suggests that a large fraction of acidic SO_4^{2-} particles observed during the sea breeze period were freshly formed in the atmosphere.

It is important to note that the period with elevated concentrations of sulfate and sulfur-containing fragments were synchronized with the sea breeze from the southwest, from which refineries, petrochemical industries and shipping emissions could be carried to our sampling site (Figure 2 and S6e). Therefore, the enhancements of sulfate and organo-sulfur could be due to oxidation of biogenic dimethyl sulfide (DMS) emitted from the ocean which can produce methylsulfonic acid (MSA) and SO_4^{2-} (Ge et al., 2012; Willis et al., 2016; Xu et al., 2017; Saarikoski et al., 2019) in addition to the local anthropogenic sources such as SO_2 emitted from shipping activities and industries (e.g., oil refinery in this study) (Saliba et al., 2010; Ripoll et al., 2015; Rivellini et al., 2017). The sulfur-containing fragments measured by the SP-AMS, including CH_3SO^+, $CH_2SO_2^+$ and $CH_3SO_2^+$ that could be attributed to both MSA and organo-sulfur compounds (Farmer et al., 2010). In particular, $CH_3SO_2^+$ fragment showed a moderate correlation with both SO_4^{2-} and less-oxidized oxygenated OA (LO-OOA, see PMF results for OA in Section 3.3) ($r = 0.66$-0.73) and the lowest $NH_4^+{}_{,meas}/NH_4^+{}_{,pred}$ values appeared to coincide with the highest values of CH_2SO^+ signals (Figure S4). ~~highlighting the possible production of organo-sulfur compounds in the acidic sulfate plumes.~~

3.3 Identification of major OA sources

Five distinct OA components were identified based on the PMF analysis of organic fragments measured by the laser-off mode of SP-AMS measurement (i.e., a standard HR-ToF-AMS measurement). The OA components include hydrocarbon-like OA (HOA), oxygenated-HOA (O-HOA), cooking-related OA (COA), less-oxidized oxygenated OA (LO-OOA) and more-oxidized oxygenated OA (MO-OOA). The mass spectra and diurnal cycles of the five OA components are presented in Figure 3. The OOA components were the main contributors to the total OA, with MO-OOA and LO-OOA accounting for 32.1 and 10.4%, respectively. The HOA, O-HOA and COA components contributed to 19.4, 26.4 and 11.7% of the total OA mass, respectively (Figure 1b). The detailed descriptions of each OA factor, classified into 1) combustion emissions, 2) cooking emissions and 3) secondary organic aerosol, are discussed in the following sections.

3.3.1 Combustion emissions

HOA was the main contributor to the POA fraction and moderately correlated with the combustion tracers including rBC (r = 0.79), NO_x (r = 0.83) and CO (r = 0.81). The mass spectrum of HOA is similar to those from engine exhausts (Crippa et al., 2013; Ng et al., 2011; Zhang et al., 2005), and is dominated by non-oxygenated fragments (i.e., C_xH_y) with an average H:C and O:C ratios of 2.12 and 0.07, respectively. HOA accounted for up to ~20% of total OA during the morning (~9:00 LT) which matched the enhancement of traffic volume during the rush hours. In addition, the concentrations of HOA started increasing at the beginning of evening rush hours (~17:00 LT) and reached the maximum at ~21:00 LT. HOA and combustion tracers (rBC, NO_x and CO) exhibited a hotspot in the NWR plots (Figure 2, S7e and f) at relatively low wind speed conditions. The above observations suggest that HOA concentrations were largely influenced by nearby on-road engine exhausts and boundary layer contraction in the evening.

High concentrations of rBC, NO_x and HOA were observed during the mid-night between May 25th and 28th, indicating the presence of large combustion sources during nighttime that might impact the air quality at our sampling site occasionally (Figure 1a). This observation also reflected from the diurnal plots (Figures 3 and S8) that the mean mass concentrations of HOA, rBC, NO_X and CO during the mid-night were much higher than their corresponding median values. Figure S8a shows that the highest N:C ratio was observed during the morning traffic peak hours but remained relatively low for the rest of the period. Such observation suggests that the emission characteristics of these unknown combustion sources at nighttime could be different to those associated with traffic emissions during the daytime. Although it is difficult to confirm the origin of those nighttime combustion emissions without further evidence, the observed events were coupled to low wind speed condition, suggesting that they were likely due to local emissions from the city. For example, significant emissions due to flaring from petrochemical industries, which largely depends on plant operation, during the relatively stagnant atmospheric condition could lead to elevated concentrations of the combustion-related species.

O-HOA showed distinctive time series and oxygenation level compared to HOA (r = 0.17, O:C = 0.07). The mass spectral profile (Figure 3) illustrate that O-HOA could be an oxygenated fraction of combustion particles which

were co-emitted with HOA and/or produced rapidly through oxidation of HOA near emission sources. However, similar to the case of rBC, the elevated concentrations of O-HOA observed from the southwest direction with strong wind speed (~18 m s^{-1}) suggests that O-HOA was partly related to the emissions transported from the industrial zone (Figure 2). The temporal variability of O-HOA depicts a rather singular behavior, showing a higher average concentration before May 24th (2.2 µg m^{-3}). During rest of the campaign, the principal source of O-HOA was mainly local anthropogenic activities (Figure S7a-d) and remained at rather low concentration with an average of 0.9 µg m^{-3}. The relatively constant diurnal cycle of O-HOA compared to that of HOA further underlines multiple sources of this OA component.

3.3.2 Cooking emissions

COA is another major POA component identified in this study. COA concentrations remained low in the morning and exhibited peaks around lunch (13:00 LT) and dinner time (21:00 LT) (Figure 3). This type of COA diurnal pattern has been commonly observed in urban studies (Allan et al., 2010; Sun et al., 2011; Fröhlich et al., 2015). Furthermore, COA mass spectrum shows a higher *m/z* 55/57 ratio than HOA as reported in previous studies (Allan et al., 2010; Mohr et al., 2012) and is strongly correlated with the COA mass spectrum reported in France (Crippa et al., 2013) and in the megacities of China (Hu et al., 2013; Elser et al., 2016). An organic fragment tracer, $C_6H_{10}O^+$, tracked the time profile of COA (r^2 = 0.90), further confirming the existence of COA components (Zhang et al., 2011). A local COA hotspot shown in the NWR plots (Figure 2) suggests that the campus canteens and residential building nearby are likely the major contributors to the observed COA mass loadings. Note that COA can contribute up to 50% of total OA in other urban locations (e.g., downtown area with substantial emissions from restaurants) depending on the site characteristics (Allan et al., 2010; Huang et al., 2010; Sun et al., 2012; Crippa et al., 2013) and cooking styles. Similar to other combustion-related emissions, high concentrations of COA component were also observed during the mid-night between May 25th and 28th (Figure 1). This observation implies that combustion-related emissions might contain some COA-like particles, contributing to the reported mass concentrations of COA in general. After removing the data from May 25th and 28th, the diurnal profile shows that lower mass concentrations of COA were observed overnight (Figure S8d).

3.3.3 Secondary organic aerosol

The mass spectra of LO-OOA was dominated by the oxygenated fragments of $C_2H_3O^+$ and CO_2^+ whereas MO-OOA was mainly characterized by CO_2^+ fragments (Figure 3). The different degree of oxygenation between LO-OOA and MO-OOA and their secondary nature are shown in the Van-Krevelen diagram (Figure S9) (Heald et al., 2010; Ng et al., 2011). MO-OOA (O:C = 0.94, N:C = 0.01) likely represented a more aged fraction of SOA. The MO-OOA concentrations were insensitive to the local wind pattern (i.e., more homogeneous distribution in the NWR plot, Figure 2) and increased gradually in the afternoon, possibly due to the combined effects of photochemistry and mixing of air masses transported from the regions without significant local industrial influences. Similar to many other studies, sources identification of MO-OOA component is not straightforward as their mass spectral features can be obtained by oxidation of different types of POA and SOA components

(Donahue et al., 2009; Jimenez et al., 2009; Zhang et al., 2007b). Additional information is essential to further interpret their potential sources and/or formation mechanisms (see discussion in Section 3.5).

In contrast, the moderate correlation observed between LO-OOA and SO_4^{2-} (r = 0.73) and the similarity between their diurnal patterns illustrate that LO-OOA were freshly formed SOA materials (O:C = 0.41). The latter might be formed via local photo-oxidation of POA and/or SOA precursors under the influences of anthropogenic emissions transported form the southwest direction due to sea breeze (Figure 2). Previous laboratory studies have evidenced the importance of acidic seeds and RH on SOA formation (Liggio and Li, 2006; Wong et al., 2015). The acidic nature of sulfate particles and RH encountered on site might facilitate the partitioning of volatile organic compounds (VOCs, from both biogenic and anthropogenic sources) into particle-phase, leading to the production of SOA and perhaps organo-sulfur compounds as discussed in Section 3.2. Furthermore, Kasthuriarachchi et al., (2020) reported that the concentrations of organo-nitrate and nitrogen-containing fragments (i.e., $C_xH_yN^+$ and $C_xH_yNO_z^+$) slightly increased during daytime (e.g., Figure S8a) with LO-OOA, contributing to 30% of observed $C_xH_yNO_z^+$ fragments (Figure S10). This suggests that photo-oxidation of VOCs under high-NO_X condition could be a potential pathway toward LO-OOA formation given that the NO_X concentrations reached up to 160 ppb (Figure 1a, mean = 16.5 ppb) during the campaign.

3.4 Characterization of rBC associated with different OA sources

Integrating rBC fragments (C_1^+–C_9^+) to the PMF analysis of organic fragments measured by the laser-on mode of SP-AMS measurements yielded a five-factor solution. They show similar mass spectra and temporal variabilities compared to their corresponding OA factors identified in the PMF analysis of the laser-off datasets (Figures S4 and S5). These observations suggest that the major OA sources identified in Section 3.3 are still valid, and hence the addition of rBC fragments in the PMF analysis can provide additional information to improve our understanding on how ambient rBC might be co-emitted or interacted with different types of POA and SOA during their atmospheric dispersion. Note that Figure S4 shows higher mass loadings of PMF factors determined by the laser-on measurement than those observed in the PMF results from the laser-off measurement. This type of OA signal enhancements has been observed in previous studies (Lee et al., 2015; Willis et al., 2014) but the fundamental reason remains unclear. Therefore, this section will primarily focus on 1) quantifying the distribution of rBC fragments among different PMF factors and 2) investigating the potential application of rBC fragment ratios for identifying the origin of ambient rBC-containing particles.

Figure 4a shows that 43% of total rBC mass was associated with the HOA components in this study, indicating that a majority of rBC were emitted by local vehicular emissions. The COA factor was associated with less than 2% of total rBC mass, suggesting that they were unlikely to be co-emitted from modern kitchens and that coalescence of COA and rBC particles was insignificant near the sampling location, which is consistent with previous studies that COA and rBC were largely externally mixed in different urban environments (Lee et al., 2015, 2017; Wang et al., 2018). This observation also suggests that the potential interferences of combustion-related emissions (Section 3.3.2) to the overall temporal variation and mass concentrations of COA are unlikely significant. The two OA components that were influenced by local industries, O-HOA and LO-OOA, were

associated with 20 and 29% of the total rBC, respectively. This result highlights the fact that both O-HOA and LO-OOA components consist of mixtures of primary and secondary particles (i.e., rBC + HOA + OOA for O-HOA and rBC + OOA for LO-OOA) although they could be influenced by different types of industrial emissions and atmospheric processing. It is worth noting that LO-OOA had the second largest contribution to the total rBC, suggesting that at least a fraction of rBC from industrial emissions could act as effective condensation sinks of LO-OOA produced via the photochemistry along their dispersion. While MO-OOA had the largest contribution to total OA mass, only 6% of the total rBC mass was associated with this aged SOA component.

Previous studies have reported that physical structure and chemical composition of BC-containing particles depend on the conditions of combustion processes and the types of combustible involved (Vander Wal and Tomasek, 2004). Such relationship is possibly observed through the relative intensities of the carbon fragments (C_1^+-C_3^+) (Corbin et al., 2014). Table 1 shows that the C_2^+/C_3^+ ratios remained roughly constant regardless of the origin of rBC, whereas the C_1^+/C_3^+ ratios varied between PMF factors. The relative contributions of each factor to C_1^+ to C_3^+ fragments are presented in Figure 4b. The C_1^+/C_3^+ ratios of rBC associated with HOA was 0.66 (±0.07) , which was within the range of those emitted from aircraft-turbine, regal black (i.e., a BC standard for SP-AMS calibration) and particles produced by a propane diffusion flame (0.50 – 0.78) and, more importantly, close to those reported for diesel engine exhaust (Carbone et al., 2019; Corbin et al., 2014; Onasch et al., 2012). Furthermore, the size distribution of unit mass resolution data shows lower *m/z* 12-to-*m/z* 36 ratios (a proxy for C_1^+/C_3^+) for particles with d_{va} smaller than 100 nm (Figure S11a). This suggests that rBC particles with relatively small diameter were mainly associated with fresh traffic emissions (Massoli et al., 2012). Our results illustrate that rBC transported from industrial area and shipping ports gave C_1^+/C_3^+ ratios closer to unity (i.e., LO-OOA = 0.79 (±0.10) and O-HOA = 1.00 (±0.11), which is similar to the previous observations for soot particles emitted from a marine engine using heavy-fuel-oil (Corbin et al., 2018), rBC-containing particles emitted from chemical and petrochemical industries (Wang et al., 2018), and rBC with high fullerene content (Canagaratna et al., 2015a; Corbin et al., 2014). The NWR and diurnal plots of C_1^+/C_3^+ ratio (Figure 4c and d) clearly show that rBC with higher C_1^+/C_3^+ ratios were transported to the site by sea breeze from the southwest direction, which are consistent with our PMF results that O-HOA and LO-OOA were influenced by industrial emissions and were associated with rBC with higher C_1^+/C_3^+ ratios compared to other OA components.

3.5 Characterization of metal ions associated with different OA sources

In addition to quantifying rBC, the laser-on mode of SP-AMS measurement can detect trace metals as rBC-containing particles can be heated to reach the temperature for vaporizing the associated trace metals (Carbone et al., 2015; Corbin et al., 2018; Onasch et al., 2012). In this work, five trace metal ions, including K^+, Rb^+, Na^+, V^+ and Ni^+, were integrated into the PMF analysis of organic and rBC fragments measured by the laser-on mode of SP-AMS. The addition of these trace metal ions did not result in major changes in the mass spectral features and temporal variations of the five PMF factors identified in Section 3.4 (Figures S4 and S5). Since these trace metals are relatively stable in the particle-phase, investigating how these trace metal ions are associated with different PMF factors can improve our understanding on the emission characteristics and perhaps the aging history of

specific OA components. This section will mainly focus on discussing the trace metals associated with OA and rBC that were associated with 1) local combustion emissions, and 2) aged SOA component (i.e., MO-OOA).

3.5.1 Combustion emissions

Based on the PMF results that includes trace metal ions, sodium (Na^+) was mainly associated with HOA, O-HOA and LO-OOA (Figure 5a) that could be due to different types of fossil fuel combustion emissions (e.g., local traffic, shipping, and various industrial activities) as discussed in Section 3.4. The Na^+ signals also correlated strongly with rBC (r = 0.80, Figure 5b) and moderately with HOA (r = 0.65). The absence of correlation between rBC and Na^+ in the laser-off mode measurement suggests a large degree of internal mixing of Na and rBC. The presence of sodium compounds in fuel, including remaining catalyst used for biodiesel esterification, drying agents, corrosion inhibitors and fuel additives, has been previously observed as a cause of fuel injectors fouling (Barker et al., 2013; Coordinating Research Council, 2013), and hence co-emissions of sodium with rBC and HOA from on-road engines was highly possible. Recent experiments conducted with SP-AMS measurements also reported non-negligible amounts of Na in soot particles emitted by marine, locomotive and vehicle engines (Dallmann et al., 2014; Omidvarborna et al., 2016; Saarikoski et al., 2017; Corbin et al., 2018; Carbone et al., 2019). Na^+ is widely used for identifying the influence of marine sources in source apportionment analysis, hence the potential contribution of sea spray aerosols to Na^+ signals cannot be neglected, especially for those factors (i.e., O-HOA and LO-OOA) connected to sea breeze transport. However, it is important to emphasize that Na^+ and Cl^- exhibit rather poor temporal correlations (r < 0.30) for both laser-off and laser-on data regardless the influences of sea breeze. Biomass burning can be a possible source of Na^+ (Hsu et al., 2011) but no major fresh biomass burning emissions were observed in this study. The MO-OOA factor is suspected to be more influenced by aged regional biomass burning emissions (see more discussion in Section 3.5.2) but Na^+ was not strongly associated with this factor.

Vanadium (V) and Nickel (Ni) are usually residual trace metals in fuel and their ratio in emissions can vary with fuel types or combustion processes (Moldanová et al., 2009; Yakubov et al., 2016). This ratio can be used to trace emissions from ship or heavy oil combustion industries (Ault et al., 2010; Liu et al., 2017). In particular, Figure 5c shows that the V^+/Ni^+ ratio exhibited a distinctive diurnal variation, with higher values from 12:00 to 18:00 LT, which coincided with the sea breeze pattern. Two maxima are observed at 13:00 and 17:00 LT with the hourly-averaged V^+/Ni^+ ratio between 5 and 7 (75th percentiles > 12) (Figure 5c). Assuming similar RIE for V^+ and Ni^+ measured by the SP-AMS, our observation is consistent with other studies, reporting that the V^+/Ni^+ ratios ranged from 4 to 7 for ship emissions and heavy fuel combustion by engines (Agrawal et al., 2009; Corbin et al., 2018; Viana et al., 2008). In addition to a moderate correlation between LO-OOA and V^+ (r = 0.47), ~70% of the V^+ signals were associated with the LO-OOA component (Figure 5a). Figure 5d clearly shows that the V^+/Ni^+ ratios increased with the concentrations of SO_4^{2-} and LO-OOA during the sea breeze from southwest direction. These observations confirm that a part of the SO_4^{2-} and LO-OOA encountered on site were influenced by ship emissions and/or heavy oil combustion from the industrial zone.

3.5.2 Potential origins of MO-OOA

Although a large local source of biomass burning in Singapore is uncommon, it is important to investigate the potential influences of biomass burning events, including agricultural burning and forest fires, from the nearby countries (Figure S12a). Budisulistiorini et al. (2018) reports high mass loadings of biomass burning OA (BBOA) during the Indonesian wildfire in 2015 which had strong impacts on the air quality in the Southeast Asia. BBOA is not identified in the PMF analysis in this field study. However, the average fraction of $C_2H_4O_2^+$ to total organic ($f_{C2H4O2+}$) of 0.8% (Figure S13a) with ~86% of the data giving $f_{C2H4O2+}$ above 0.3% (i.e., a background $f_{C2H4O2+}$ values for non-biomass burning (Cubison et al., 2011)) in the laser-off mode measurement suggests potential influences from aged biomass burning emissions that cannot be easily separated by the conventional PMF analysis of organic fragments alone. Note that MO-OOA and COA present slightly higher $f_{C2H4O2+}$ values of 0.5% and 0.8% respectively (Figure 6a). However, the origin of MO-OOA is highly uncertain compared to other OA factors identified in this study due to the fact that atmospheric aging can diminish the distinctive mass spectral features of POA in general (e.g., decreasing in $f_{C2H4O2+}$ for BBOA (Cubison et al., 2011) and converging in the f_{43}-f_{44} framework for OOA production (Ng et al. 2010)). Therefore, the following discussion will focus on evaluating the potential connections between the MO-OOA component and aged regional emissions.

Figures 6c and S14b show that high Rb^+ and K^+ signals were associated with more oxygenated (f_{44} > 0.7) fraction of OA, and moderate correlations between MO-OOA and the two metal were observed (Rb^+, r = 0.58 and K^+, r = 0.71, Figure S13b). Furthermore, the results of PMF analysis demonstrated that both K^+ and Rb^+ were mainly associated with MO-OOA (58-66%, Figure 5a) followed by the two combustion-related components (HOA and O-HOA). Although potassium and rubidium are not unique tracers for a specific combustion source, previous studies have shown that these two metals can be largely associated with biomass burning emissions (Artaxo et al., 1993; Lee et al., 2016; Achad et al., 2018). Note that rubidium has also been used as a coal combustion tracer in previous studies (Fine et al., 2004; Irei et al., 2014). Unlike ambient OA component, the chemical identities of K^+ and Rb^+ are unlikely modified by the oxidative aging of aerosol particles. Therefore, a strong temporal correlation between Rb^+ and K^+ (r = 0.85, Figure 6b) further suggests that they were likely of similar origins in this study.

The regional origin of K^+, Rb^+, $C_2H_4O_2^+$ and MO-OOA were investigated through their PSCF. Their PSCF graphs (Figures 6d and S15a- c) show several common origins with high probability that the highest concentrations could be influenced by biomass burning events from Indonesia (Figure S12a). Nevertheless, coal-fired power plants are located nearby the identified hotspots of Rb^+ and K^+ (Figure S12b) so that a regional transport of coal-fired power plant emissions alongside biomass burning plumes were possible. Note that MO-OOA contributes to the highest fraction of nitrogen-containing organic fragments ($C_xH_yNO_z^+$ ~ 32% and $C_xH_yN^+$ ~ 46%) that can be generated by biomass burning emissions (Mace et al., 2003; Laskin et al., 2009; Desyaterik et al., 2013; Mohr et al., 2013). It is important to point out that most of the previous studies usually describe MO-OOA (or LV-OOA in some earlier studies) as aged SOA component without providing further detail on their potential origin and emission characteristics. Our observations underline the possibility of better understanding the origin of the MO-OOA component through measurements of refractory metals even when atmospheric oxidative processing has made the mass spectral features of aged OA materials less distinguishable.

4. Conclusions and Atmospheric Implications

Real-time aerosol mass spectrometry techniques have been successfully deployed in the fields worldwide in the last two decades and their observations have substantially enhanced our quantitative understanding of sources and formation of NR-PM, in particular through the use of PMF analysis for OA source apportionment (Fröhlich et al., 2015; Ng et al., 2010; Zhang et al., 2007b). In this work, we demonstrate the use of refractory aerosol components, rBC and a few trace metals, measured by an Aerodyne SP-AMS to better characterize the sources, emission characteristics and aging history of ambient OA and rBC in Singapore, a highly urbanized tropical city that is influenced by multiple local and regional air pollution sources.

By integrating rBC fragment (C_n^+) into the PMF analysis, we can identify the major sources and characteristics of ambient rBC and OA particles based on their degree of associations. In particular, the majority of total rBC (> 90%) was originated from local combustion emissions, in which ~30% of them were largely associated with the fresh SOA components (LO-OOA). This observation implies that a fraction of rBC could act as condensation sinks of fresh SOA in this field study although additional information is required to determine the mixing state of rBC and SOA. We further illustrate the potential application of relative intensities of major rBC fragments for aerosol source identification. While higher C_1^+/C_3^+ ratios (> 0.7) were associated with rBC originated from the industrial zone and shipping port (O-HOA and LO-OOA), rBC associated with traffic (HOA) gave lower C_1^+/C_3^+ ratios (~0.65). Trace metals analysis further shows that the high C_1^+/C_3^+ ratios coincided with high V^+/Ni^+ ratios, highlighting the potential influences of emission from shipping activities and oil refinery industry on the chemical characteristics of O-HOA and LO-OOA. The observed correlation between Na^+ and rBC suggests that the contribution of anthropogenic emissions to total particulate sodium should not be ignored in the coastal urban environments. These results underline the advantages of using refractory aerosol component to disentangle various combustion sources encountered in an urban environment influenced by multiple sources using a single online instrument.

One of the major challenges in interpreting the PMF results from AMS measurements is to identify the origin and aging history of ambient particles associated with highly oxidized OA components (e.g., MO-OOA in this work), as the mass spectral characteristics of OA converge along with their degree of oxidative aging. In general, the relative intensities of some highly oxygenated fragments (e.g. CO^+ and CO_2^+) increase continuously while other mass spectral features (e.g. alkane/alkene patterns from combustion sources) being diminished during the aging processes. Ng et al. (2010) have visualized such phenomena for SOA components on the f_{43}-f_{44} space. Furthermore, the *m/z* 60 (or $C_2H_4O_2^+$ organic fragments) has been widely used as a tracer ions for BBOA. Cubison et al. (2011) have generalized observations from worldwide field data that *m/z* 60 signature become less and less significant in aged BBOA materials. In this study, we proposed that the MO-OOA component represented aged OA materials impacted by the regional biomass burning and perhaps coal combustion emissions as MO-OOA was associated with refractory K^+ and Rb^+. Given the fact that MO-OOA was the major OA components of the total OA (~32%), this result highlights the fact that the regional pollution can affect the air quality in Singapore even though fresh regional biomass burning episodes were not observed during the sampling period.

More broadly, the improved source identification for OA and rBC can provide useful information to further investigate the effects of atmospheric aging on their physio-chemical properties. For example, this work highlights

the potential influences of regional biomass burning and coal combustion emissions to MO-OOA component, which may provide important insight into how light absorbing properties of OA (i.e., brown carbon) evolve with transport and aging. Recently, Dasari et al. (2019) provided field evidence for the bleaching of brown carbon during their transport by photo-oxidation and that photo-dissociation can occur in the South Asian outflow based on measurements near and away from specific combustion sources, including biomass burning and traffic. Furthermore, this type of PMF analysis could be applied to analyze the sources and characteristics of rBC-containing particles exclusively (i.e., rBC core with organic coatings) in order to advance our understanding on the effects of primary emissions and/or atmospheric processing on BC light absorption enhancement caused by the lensing effect.

Acknowledgment: This work is supported by the National Environmental Agency (NEA) of Singapore (NEA, R-706-000-043-490) and by the National University of Singapore start-up grant (R-302-000-173-133). The content does not represent NEA's view.

Author contributions: A.K.Y.L. supervised the project. M.G.A. and N.K. carried out the experiment. L.-H.R. and M.G.A analysed the data. L.-H.R. wrote the manuscript with support and comments from all the co-authors.

References

Achad, M., Caumo, S., de Castro Vasconcellos, P., Bajano, H., Gómez, D. and Smichowski, P.: Chemical markers of biomass burning: Determination of levoglucosan, and potassium in size-classified atmospheric aerosols collected in Buenos Aires, Argentina by different analytical techniques, Microchem. J., 139, 181–187, doi:10.1016/j.microc.2018.02.016, 2018.

Agrawal, H., Eden, R., Zhang, X., Fine, P. M., Katzenstein, A., Miller, J. W., Ospital, J., Teffera, S. and Cocker, D. R.: Primary Particulate Matter from Ocean-Going Engines in the Southern California Air Basin, Environ. Sci. Technol., 43(14), 5398–5402, doi:10.1021/es8035016, 2009.

Allan, J. D., Bower, K. N., Coe, H., Boudries, H., Jayne, J. T., Caragaratna, M. R., Millet, D. B., Goldstein, A. H., Quinn, P. K., Weber, R. J. C. G. L. and Worsnop, D. R.: Submicron aerosol composition at Trinidad Head, California, during ITCT 2K2: Its relationship with gas phase volatile organic carbon and assessment of instrument performance, J. Aerosol Sci., 35, 909–922, doi:10.1016/j.jaerosci.2004.02.007, 2004.

Allan, J. D., Williams, P. I., Morgan, W. T., Martin, C. L., Flynn, M. J., Lee, J., Nemitz, E., Phillips, G. J., Gallagher, M. W. and Coe, H.: Contributions from transport, solid fuel burning and cooking to primary organic aerosols in two UK cities, Atmospheric Chem. Phys., 10(2), 647–668, doi:https://doi.org/10.5194/acp-10-647-2010, 2010.

Artaxo, P., Gerab, F. and Rabello, M. L.: Elemental composition of aerosol particles from two atmospheric monitoring stations in the Amazon Basin, Nucl. Instrum. Methods Phys. Res. Sect. B Beam Interact. Mater. At., 75(1–4), 277–281, 1993.

Attwood, A. R., Washenfelder, R. A., Brock, C. A., Hu, W., Baumann, K., Campuzano-Jost, P., Day, D. A., Edgerton, E. S., Murphy, D. M., Palm, B. B., McComiskey, A., Wagner, N. L., Sá, S. S. de, Ortega, A., Martin, S. T., Jimenez, J. L. and Brown, S. S.: Trends in sulfate and organic aerosol mass in the Southeast U.S.: Impact on aerosol optical depth and radiative forcing, Geophys. Res. Lett., 41(21), 7701–7709, doi:10.1002/2014GL061669, 2014.

Atwood, S. A., Reid, J. S., Kreidenweis, S. M., Yu, L. E., Salinas, S. V., Chew, B. N. and Balasubramanian, R.: Analysis of source regions for smoke events in Singapore for the 2009 El Nino burning season, Atmos. Environ., 78, 219–230, doi:10.1016/j.atmosenv.2013.04.047, 2013.

Ault, A. P., Gaston, C. J., Wang, Y., Dominguez, G., Thiemens, M. H. and Prather, K. A.: Characterization of the Single Particle Mixing State of Individual Ship Plume Events Measured at the Port of Los Angeles, Environ. Sci. Technol., 44(6), 1954–1961, doi:10.1021/es902985h, 2010.

Baker, J.: A cluster analysis of long range air transport pathways and associated pollutant concentrations within the UK, Atmos. Environ., 44(4), 563–571, doi:10.1016/j.atmosenv.2009.10.030, 2010.

Balasubramanian, R. and Qian, W.-B.: Characterization and source identification of airborne trace metals in Singapore, J. Environ. Monit., 6(10), 813–818, doi:10.1039/B407523D, 2004.

Barker, J., Cook, S. and Richards, P.: Sodium Contamination of Diesel Fuel, its Interaction with Fuel Additives and the Resultant Effects on Filter Plugging and Injector Fouling, SAE Int. J. Fuels Lubr., 6(3), 826–838, doi:10.4271/2013-01-2687, 2013.

Borge, R., Lumbreras, J., Vardoulakis, S., Kassomenos, P. and Rodríguez, E.: Analysis of long-range transport influences on urban PM10 using two-stage atmospheric trajectory clusters, Atmos. Environ., 41(21), 4434–4450, doi:10.1016/j.atmosenv.2007.01.053, 2007.

Budisulistiorini, S. H., Riva, M., Williams, M., Miyakawa, T., Chen, J., Itoh, M., Surratt, J. D. and Kuwata, M.: Dominant contribution of oxygenated organic aerosol to haze particles from real-time observation in Singapore during an Indonesian wildfire event in 2015, Atmospheric Chem. Phys., 18(22), 16481–16498, doi:https://doi.org/10.5194/acp-18-16481-2018, 2018.

Canagaratna, M. R., Massoli, P., Browne, E. C., Franklin, J. P., Wilson, K. R., Onasch, T. B., Kirchstetter, T. W., Fortner, E. C., Kolb, C. E., Jayne, J. T., Kroll, J. H. and Worsnop, D. R.: Chemical Compositions of Black Carbon

Particle Cores and Coatings via Soot Particle Aerosol Mass Spectrometry with Photoionization and Electron Ionization, J. Phys. Chem. A, 119(19), 4589–4599, doi:10.1021/jp510711u, 2015a.

Canagaratna, M. R., Jimenez, J. L., Kroll, J. H., Chen, Q., Kessler, S. H., Massoli, P., Hildebrandt Ruiz, L., Fortner, E., Williams, L. R., Wilson, K. R., Surratt, J. D., Donahue, N. M., Jayne, J. T. and Worsnop, D. R.: Elemental ratio measurements of organic compounds using aerosol mass spectrometry: characterization, improved calibration, and implications, Atmos Chem Phys, 15(1), 253–272, doi:10.5194/acp-15-253-2015, 2015b.

Carbone, S., Onasch, T., Saarikoski, S., Timonen, H., Saarnio, K., Sueper, D., Rönkkö, T., Pirjola, L., Häyrinen, A., Worsnop, D. and Hillamo, R.: Characterization of trace metals on soot aerosol particles with the SP-AMS: detection and quantification, Atmos Meas Tech, 8(11), 4803–4815, doi:10.5194/amt-8-4803-2015, 2015.

Carbone, S., Timonen, H. J., Rostedt, A., Happonen, M., Rönkkö, T., Keskinen, J., Ristimaki, J., Korpi, H., Artaxo, P., Canagaratna, M., Worsnop, D., Canonaco, F., Prévôt, A. S. H., Hillamo, R. and Saarikoski, S.: Distinguishing fuel and lubricating oil combustion products in diesel engine exhaust particles, Aerosol Sci. Technol., 0(0), 1–14, doi:10.1080/02786826.2019.1584389, 2019.

Chou, L. M., Huang, D., Tan, K. S., Toh, T. C., Goh, B. P. L. and Tun, K.: Chapter 24 - Singapore, in World Seas: an Environmental Evaluation (Second Edition), edited by C. Sheppard, pp. 539–558, Academic Press., 2019.

Coordinating Research Council: CRC Report No. 665: Internal Diesel Injector Deposits, Coordinating Research Council, inc., [online] Available from: www.crcao. org/reports/recentstudies2013/DP-04-13a%20 CRC%20665/CRC%20665.pdf, 2013.

Corbin, J. C., Sierau, B., Gysel, M., Laborde, M., Keller, A., Kim, J., Petzold, A., Onasch, T. B., Lohmann, U. and Mensah, A. A.: Mass spectrometry of refractory black carbon particles from six sources: carbon-cluster and oxygenated ions, Atmos Chem Phys, 14(5), 2591–2603, doi:10.5194/acp-14-2591-2014, 2014.

Corbin, J. C., Mensah, A. A., Pieber, S. M., Orasche, J., Michalke, B., Zanatta, M., Czech, H., Massabò, D., Buatier de Mongeot, F., Mennucci, C., El Haddad, I., Kumar, N. K., Stengel, B., Huang, Y., Zimmermann, R., Prévôt, A. S. H. and Gysel, M.: Trace Metals in Soot and PM $_{2.5}$ from Heavy-Fuel-Oil Combustion in a Marine Engine, Environ. Sci. Technol., 52(11), 6714–6722, doi:10.1021/acs.est.8b01764, 2018.

Crippa, M., DeCarlo, P., Slowik, J., Mohr, C., Heringa, M., Chirico, R., Poulain, L., Freutel, F., Sciare, J. and Cozic, J.: Wintertime aerosol chemical composition and source apportionment of the organic fraction in the metropolitan area of Paris, Atmospheric Chem. Phys., 13(2), 961–981, 2013.

Cubison, M. J., Ortega, A. M., Hayes, P. L., Farmer, D. K., Day, D., Lechner, M. J., Brune, W. H., Apel, E., Diskin, G. S., Fisher, J. A., Fuelberg, H. E., Hecobian, A., Knapp, D. J., Mikoviny, T., Riemer, D., Sachse, G. W., Sessions, W., Weber, R. J., Weinheimer, A. J., Wisthaler, A. and Jimenez, J. L.: Effects of aging on organic aerosol from open biomass burning smoke in aircraft and laboratory studies, Atmos Chem Phys, 11(23), 12049–12064, doi:10.5194/acp-11-12049-2011, 2011.

Dallmann, T. R., Onasch, T. B., Kirchstetter, T. W., Worton, D. R., Fortner, E. C., Herndon, S. C., Wood, E. C., Franklin, J. P., Worsnop, D. R., Goldstein, A. H. and Harley, R. A.: Characterization of particulate matter emissions from on-road gasoline and diesel vehicles using a soot particle aerosol mass spectrometer, Atmospheric Chem. Phys., 14(14), 7585–7599, doi:https://doi.org/10.5194/acp-14-7585-2014, 2014.

Dasari, S., Andersson, A., Bikkina, S., Holmstrand, H., Budhavant, K., Satheesh, S., Asmi, E., Kesti, J., Backman, J., Salam, A., Bisht, D. S., Tiwari, S., Hameed, Z. and Gustafsson, Ö.: Photochemical degradation affects the light absorption of water-soluble brown carbon in the South Asian outflow, Sci. Adv., 5(1), eaau8066, doi:10.1126/sciadv.aau8066, 2019.

DeCarlo, P. F., Kimmel, J. R., Trimborn, A., Northway, M. J., Jayne, J. T., Aiken, A. C., Gonin, M., Fuhrer, K., Horvath, T., Docherty, K. S., Worsnop, D. R. and Jimenez, J. L.: Field-Deployable, High-Resolution, Time-of-Flight Aerosol Mass Spectrometer, Anal. Chem., 78(24), 8281–8289, doi:10.1021/ac061249n, 2006.

Desyaterik, Y., Sun, Y., Shen, X., Lee, T., Wang, X., Wang, T. and Collett, J. L.: Speciation of "brown" carbon in cloud water impacted by agricultural biomass burning in eastern China, J. Geophys. Res. Atmospheres, 118(13), 7389–7399, doi:10.1002/jgrd.50561, 2013.

Diez, J. R., Breul, M. and Moneke, J.: The SIJORI Growth Triangle: Territorial Complementarities or Competition for FDI in the Oil and Gas Industry?, J. Southeast Asian Econ. JSEAE, 36(1), 71–90, 2019.

Donahue, N. M., Robinson, A. L. and Pandis, S. N.: Atmospheric organic particulate matter: From smoke to secondary organic aerosol, Atmos. Environ., 43(1), 94–106, doi:10.1016/j.atmosenv.2008.09.055, 2009.

Draxler, R. R. and Rolph, G.: HYSPLIT (HYbrid Single-Particle Lagrangian Integrated Trajectory) model access via NOAA ARL READY website (http://www. arl. noaa. gov/ready/hysplit4. html). NOAA Air Resources Laboratory, Silver Spring, 2003.

Elser, M., Huang, R.-J., Wolf, R., Slowik, J. G., Wang, Q., Canonaco, F., Li, G., Bozzetti, C., Daellenbach, K. R., Huang, Y., Zhang, R., Li, Z., Cao, J., Baltensperger, U., El-Haddad, I. and Prévôt, A. S. H.: New insights into PM2.5 chemical composition and sources in two major cities in China during extreme haze events using aerosol mass spectrometry, Atmos Chem Phys, 16(5), 3207–3225, doi:10.5194/acp-16-3207-2016, 2016.

Engling, G., He, J., Betha, R. and Balasubramanian, R.: Assessing the regional impact of indonesian biomass burning emissions based on organic molecular tracers and chemical mass balance modeling, Atmospheric Chem. Phys., 14(15), 8043–8054, doi:https://doi.org/10.5194/acp-14-8043-2014, 2014.

Farmer, D. K., Matsunaga, A., Docherty, K. S., Surratt, J. D., Seinfeld, J. H., Ziemann, P. J. and Jimenez, J. L.: Response of an aerosol mass spectrometer to organonitrates and organosulfates and implications for atmospheric chemistry, Proc. Natl. Acad. Sci., 107(15), 6670–6675, doi:10.1073/pnas.0912340107, 2010.

Fine, P. M., Cass, G. R. and Simoneit, B. R. T.: Chemical Characterization of Fine Particle Emissions from the Wood Stove Combustion of Prevalent United States Tree Species, Environ. Eng. Sci., 21(6), 705–721, doi:10.1089/ees.2004.21.705, 2004.

Fröhlich, R., Crenn, V., Setyan, A., Belis, C. A., Canonaco, F., Favez, O., Riffault, V., Slowik, J. G., Aas, W., Aijälä, M., Alastuey, A., Artiñano, B., Bonnaire, N., Bozzetti, C., Bressi, M., Carbone, C., Coz, E., Croteau, P. L., Cubison, M. J., Esser-Gietl, J. K., Green, D. C., Gros, V., Heikkinen, L., Herrmann, H., Jayne, J. T., Lunder, C. R., Minguillón, M. C., Močnik, G., O'Dowd, C. D., Ovadnevaite, J., Petralia, E., Poulain, L., Priestman, M., Ripoll, A., Sarda-Estève, R., Wiedensohler, A., Baltensperger, U., Sciare, J. and Prévôt, A. S. H.: ACTRIS ACSM intercomparison – Part 2: Intercomparison of ME-2 organic source apportionment results from 15 individual, co-located aerosol mass spectrometers, Atmos Meas Tech, 8(6), 2555–2576, doi:10.5194/amt-8-2555-2015, 2015.

Ge, X., Setyan, A., Sun, Y. and Zhang, Q.: Primary and secondary organic aerosols in Fresno, California during wintertime: Results from high resolution aerosol mass spectrometry, J. Geophys. Res. Atmospheres, 117(D19), doi:10.1029/2012JD018026, 2012.

Guo, H., Xu, L., Bougiatioti, A., Cerully, K. M., Capps, S. L., Hite Jr., J. R., Carlton, A. G., Lee, S.-H., Bergin, M. H., Ng, N. L., Nenes, A. and Weber, R. J.: Fine-particle water and pH in the southeastern United States, Atmospheric Chem. Phys., 15(9), 5211–5228, doi:https://doi.org/10.5194/acp-15-5211-2015, 2015.

Heald, C. L., Kroll, J. H., Jimenez, J. L., Docherty, K. S., DeCarlo, P. F., Aiken, A. C., Chen, Q., Martin, S. T., Farmer, D. K. and Artaxo, P.: A simplified description of the evolution of organic aerosol composition in the atmosphere, Geophys. Res. Lett., 37(8), doi:10.1029/2010GL042737, 2010.

Henry, R., Norris, G. A., Vedantham, R. and Turner, J. R.: Source Region Identification Using Kernel Smoothing, Environ. Sci. Technol., 43(11), 4090–4097, doi:10.1021/es8011723, 2009.

Hsu, L.-J., Alwahabi, Z. T., Nathan, G. J., Li, Y., Li, Z. S. and Aldén, M.: Sodium and Potassium Released from Burning Particles of Brown Coal and Pine Wood in a Laminar Premixed Methane Flame Using Quantitative Laser-Induced Breakdown Spectroscopy:, Appl. Spectrosc., doi:10.1366/10-06108, 2011.

Hu, W. W., Hu, M., Yuan, B., Jimenez, J. L., Tang, Q., Peng, J. F., Hu, W., Shao, M., Wang, M., Zeng, L. M., Wu, Y. S., Gong, Z. H., Huang, X. F. and He, L. Y.: Insights on organic aerosol aging and the influence of coal

combustion at a regional receptor site of central eastern China, Atmos Chem Phys, 13(19), 10095–10112, doi:10.5194/acp-13-10095-2013, 2013.

Huang, X.-F., He, L.-Y., Hu, M., Canagaratna, M. R., Sun, Y., Zhang, Q., Zhu, T., Xue, L., Zeng, L.-W., Liu, X.-G., Zhang, Y.-H., Jayne, J. T., Ng, N. L. and Worsnop, D. R.: Highly time-resolved chemical characterization of atmospheric submicron particles during 2008 Beijing Olympic Games using an Aerodyne High-Resolution Aerosol Mass Spectrometer, Atmospheric Chem. Phys., 10(18), 8933–8945, doi:https://doi.org/10.5194/acp-10-8933-2010, 2010.

Irei, S., Shimono, A., Hikida, T., Kuramoto, K., Suzuki, Y. and Takami, A.: Qualitative Evaluation of m/z 85, 87, and 133 Signals in Organic Aerosol Mass Spectra of Fly Ash Produced by Coal Combustion, Aerosol Air Qual. Res., 14(1), 406–412, doi:10.4209/aaqr.2013.04.0126, 2014.

Jayne, J. T., Leard, D. C., Zhang, X., Davidovits, P., Smith, K. A., Kolb, C. E. and Worsnop, D. R.: Development of an Aerosol Mass Spectrometer for Size and Composition Analysis of Submicron Particles, Aerosol Sci. Technol., 33(1–2), 49–70, doi:10.1080/027868200410840, 2000.

Jimenez, J. L.: Ambient aerosol sampling using the Aerodyne Aerosol Mass Spectrometer, J. Geophys. Res., 108(D7), doi:10.1029/2001JD001213, 2003.

Jimenez, J. L., Canagaratna, M. R., Donahue, N. M., Prevot, A. S. H., Zhang, Q., Kroll, J. H., DeCarlo, P. F., Allan, J. D., Coe, H., Ng, N. L., Aiken, A. C., Docherty, K. S., Ulbrich, I. M., Grieshop, A. P., Robinson, A. L., Duplissy, J., Smith, J. D., Wilson, K. R., Lanz, V. A., Hueglin, C., Sun, Y. L., Tian, J., Laaksonen, A., Raatikainen, T., Rautiainen, J., Vaattovaara, P., Ehn, M., Kulmala, M., Tomlinson, J. M., Collins, D. R., Cubison, M. J., E, Dunlea, J., Huffman, J. A., Onasch, T. B., Alfarra, M. R., Williams, P. I., Bower, K., Kondo, Y., Schneider, J., Drewnick, F., Borrmann, S., Weimer, S., Demerjian, K., Salcedo, D., Cottrell, L., Griffin, R., Takami, A., Miyoshi, T., Hatakeyama, S., Shimono, A., Sun, J. Y., Zhang, Y. M., Dzepina, K., Kimmel, J. R., Sueper, D., Jayne, J. T., Herndon, S. C., Trimborn, A. M., Williams, L. R., Wood, E. C., Middlebrook, A. M., Kolb, C. E., Baltensperger, U. and Worsnop, D. R.: Evolution of Organic Aerosols in the Atmosphere, Science, 326(5959), 1525–1529, doi:10.1126/science.1180353, 2009.

Kasthuriarachchi, N. Y., Rivellini, L.-H., Adam, M. G. and Lee, A. K. Y.: Strongly absorptive primary and secondary brown carbon in an urban, under review, Environ Sci Technol, 2020.

Kim, P. S., Jacob, D. J., Fisher, J. A., Travis, K., Yu, K., Zhu, L., Yantosca, R. M., Sulprizio, M. P., Jimenez, J. L., Campuzano-Jost, P., Froyd, K. D., Liao, J., Hair, J. W., Fenn, M. A., Butler, C. F., Wagner, N. L., Gordon, T. D., Welti, A., Wennberg, P. O., Crounse, J. D., Clair, J. M. S., Teng, A. P., Millet, D. B., Schwarz, J. P., Markovic, M. Z. and Perring, A. E.: Sources, seasonality, and trends of southeast US aerosol: an integrated analysis of surface, aircraft, and satellite observations with the GEOS-Chem chemical transport model, Atmospheric Chem. Phys., 15(18), 10411–10433, doi:https://doi.org/10.5194/acp-15-10411-2015, 2015.

Laskin, A., Smith, J. S. and Laskin, J.: Molecular Characterization of Nitrogen-Containing Organic Compounds in Biomass Burning Aerosols Using High-Resolution Mass Spectrometry, Environ. Sci. Technol., 43(10), 3764–3771, doi:10.1021/es803456n, 2009.

Lee, A. K. Y., Willis, M. D., Healy, R. M., Onasch, T. B. and Abbatt, J. P. D.: Mixing state of carbonaceous aerosol in an urban environment: single particle characterization using the soot particle aerosol mass spectrometer (SP-AMS), Atmos Chem Phys, 15(4), 1823–1841, doi:10.5194/acp-15-1823-2015, 2015.

Lee, A. K. Y., Willis, M. D., Healy, R. M., Wang, J. M., Jeong, C.-H., Wenger, J. C., Evans, G. J. and Abbatt, J. P. D.: Single-particle characterization of biomass burning organic aerosol (BBOA): evidence for non-uniform mixing of high molecular weight organics and potassium, Atmos Chem Phys, 16(9), 5561–5572, doi:10.5194/acp-16-5561-2016, 2016.

Lee, A. K. Y., Chen, C.-L., Liu, J., Price, D. J., Betha, R., Russell, L. M., Zhang, X. and Cappa, C. D.: Formation of secondary organic aerosol coating on black carbon particles near vehicular emissions, Atmos Chem Phys Discuss, 2017, 1–20, doi:10.5194/acp-2017-665, 2017.

Liggio, J. and Li, S.-M.: Organosulfate formation during the uptake of pinonaldehyde on acidic sulfate aerosols, Geophys. Res. Lett., 33(13), doi:10.1029/2006GL026079, 2006.

Liu, Z., Lu, X., Feng, J., Fan, Q., Zhang, Y. and Yang, X.: Influence of Ship Emissions on Urban Air Quality: A Comprehensive Study Using Highly Time-Resolved Online Measurements and Numerical Simulation in Shanghai, Environ. Sci. Technol., 51(1), 202–211, doi:10.1021/acs.est.6b03834, 2017.

Mace, K. A., Artaxo, P. and Duce, R. A.: Water-soluble organic nitrogen in Amazon Basin aerosols during the dry (biomass burning) and wet seasons, J. Geophys. Res. Atmospheres, 108(D16), doi:10.1029/2003JD003557, 2003.

Massoli, P., Fortner, E. C., Canagaratna, M. R., Williams, L. R., Zhang, Q., Sun, Y., Schwab, J. J., Trimborn, A., Onasch, T. B., Demerjian, K. L., Kolb, C. E., Worsnop, D. R. and Jayne, J. T.: Pollution Gradients and Chemical Characterization of Particulate Matter from Vehicular Traffic near Major Roadways: Results from the 2009 Queens College Air Quality Study in NYC, Aerosol Sci. Technol., 46(11), 1201–1218, doi:10.1080/02786826.2012.701784, 2012.

Middlebrook, A. M., Bahreini, R., Jimenez, J. L. and Canagaratna, M. R.: Evaluation of Composition-Dependent Collection Efficiencies for the Aerodyne Aerosol Mass Spectrometer using Field Data, Aerosol Sci. Technol., 46(3), 258–271, doi:10.1080/02786826.2011.620041, 2012.

Mohr, C., DeCarlo, P. F., Heringa, M. F., Chirico, R., Slowik, J. G., Richter, R., Reche, C., Alastuey, A., Querol, X., Seco, R., Peñuelas, J., Jiménez, J. L., Crippa, M., Zimmermann, R., Baltensperger, U. and Prévôt, A. S. H.: Identification and quantification of organic aerosol from cooking and other sources in Barcelona using aerosol mass spectrometer data, Atmos Chem Phys, 12(4), 1649–1665, doi:10.5194/acp-12-1649-2012, 2012.

Mohr, C., Lopez-Hilfiker, F. D., Zotter, P., Prévôt, A. S. H., Xu, L., Ng, N. L., Herndon, S. C., Williams, L. R., Franklin, J. P., Zahniser, M. S., Worsnop, D. R., Knighton, W. B., Aiken, A. C., Gorkowski, K. J., Dubey, M. K., Allan, J. D. and Thornton, J. A.: Contribution of Nitrated Phenols to Wood Burning Brown Carbon Light Absorption in Detling, United Kingdom during Winter Time, Environ. Sci. Technol., 47(12), 6316–6324, doi:10.1021/es400683v, 2013.

Moldanová, J., Fridell, E., Popovicheva, O., Demirdjian, B., Tishkova, V., Faccinetto, A. and Focsa, C.: Characterisation of particulate matter and gaseous emissions from a large ship diesel engine, Atmos. Environ., 43(16), 2632–2641, doi:10.1016/j.atmosenv.2009.02.008, 2009.

NEA: Annual Climatological report 2018, Scientific report, Meteorological Service Singapore. [online] Available from: http://www.weather.gov.sg/wp-content/uploads/2019/03/Annual-Climatological-Report-2018.pdf, 2018.

Ng, N. L., Canagaratna, M. R., Zhang, Q., Jimenez, J. L., Tian, J., Ulbrich, I. M., Kroll, J. H., Docherty, K. S., Chhabra, P. S., Bahreini, R., Murphy, S. M., Seinfeld, J. H., Hildebrandt, L., Donahue, N. M., DeCarlo, P. F., Lanz, V. A., Prévôt, A. S. H., Dinar, E., Rudich, Y. and Worsnop, D. R.: Organic aerosol components observed in Northern Hemispheric datasets from Aerosol Mass Spectrometry, Atmos Chem Phys, 10(10), 4625–4641, doi:10.5194/acp-10-4625-2010, 2010.

Ng, N. L., Canagaratna, M. R., Jimenez, J. L., Zhang, Q., Ulbrich, I. M. and Worsnop, D. R.: Real-Time Methods for Estimating Organic Component Mass Concentrations from Aerosol Mass Spectrometer Data, Environ. Sci. Technol., 45(3), 910–916, doi:10.1021/es102951k, 2011.

Omidvarborna, H., Kumar, A. and Kim, D.-S.: Variation of diesel soot characteristics by different types and blends of biodiesel in a laboratory combustion chamber, Sci. Total Environ., 544, 450–459, doi:10.1016/j.scitotenv.2015.11.076, 2016.

Onasch, T. B., Trimborn, A., Fortner, E. C., Jayne, J. T., Kok, G. L., Williams, L. R., Davidovits, P. and Worsnop, D. R.: Soot Particle Aerosol Mass Spectrometer: Development, Validation, and Initial Application, Aerosol Sci. Technol., 46(7), 804–817, doi:10.1080/02786826.2012.663948, 2012.

Petit, J.-E., Favez, O., Albinet, A. and Canonaco, F.: A user-friendly tool for comprehensive evaluation of the geographical origins of atmospheric pollution: Wind and trajectory analyses, Environ. Model. Softw., 88, 183–187, doi:10.1016/j.envsoft.2016.11.022, 2017.

Polissar, A. V., Hopke, P. K. and Poirot, R. L.: Atmospheric Aerosol over Vermont: Chemical Composition and Sources, Environ. Sci. Technol., 35(23), 4604–4621, doi:10.1021/es0105865, 2001.

Ripoll, A., Minguillón, M. C., Pey, J., Jimenez, J. L., Day, D. A., Sosedova, Y., Canonaco, F., Prévôt, A. S. H., Querol, X. and Alastuey, A.: Long-term real-time chemical characterization of submicron aerosols at Montsec (southern Pyrenees, 1570 m a.s.l.), Atmos Chem Phys, 15(6), 2935–2951, doi:10.5194/acp-15-2935-2015, 2015.

Rivellini, L.-H., Chiapello, I., Tison, E., Fourmentin, M., Féron, A., Diallo, A., N'Diaye, T., Goloub, P., Canonaco, F., Prévôt, A. S. H. and Riffault, V.: Chemical characterization and source apportionment of submicron aerosols measured in Senegal during the 2015 SHADOW campaign, Atmos Chem Phys, 17(17), 10291–10314, doi:10.5194/acp-17-10291-2017, 2017.

Saarikoski, S., Timonen, H., Carbone, S., Kuuluvainen, H., Niemi, J. V., Kousa, A., Rönkkö, T., Worsnop, D., Hillamo, R. and Pirjola, L.: Investigating the chemical species in submicron particles emitted by city buses, Aerosol Sci. Technol., 51(3), 317–329, doi:10.1080/02786826.2016.1261992, 2017.

Saarikoski, S., Reyes, F., Vázquez, Y., Tagle, M., Timonen, H., Aurela, M., Carbone, S., Worsnop, D. R., Hillamo, R. and Oyola, P.: Characterization of submicron aerosol chemical composition and sources in the coastal area of Central Chile, Atmos. Environ., 199, 391–401, doi:10.1016/j.atmosenv.2018.11.040, 2019.

Saliba, N. A., El Jam, F., El Tayar, G., Obeid, W. and Roumie, M.: Origin and variability of particulate matter (PM10 and PM2.5) mass concentrations over an Eastern Mediterranean city, Atmospheric Res., 97(1), 106–114, doi:10.1016/j.atmosres.2010.03.011, 2010.

Salinas, S. V., Chew, B. N., Miettinen, J., Campbell, J. R., Welton, E. J., Reid, J. S., Yu, L. E. and Liew, S. C.: Physical and optical characteristics of the October 2010 haze event over Singapore: A photometric and lidar analysis, Atmospheric Res., 122, 555–570, doi:10.1016/j.atmosres.2012.05.021, 2013.

Saputra, H., Maimun, A. and Koto, J.: Estimation and Distribution of Exhaust Ship Emission from Marine Traffic in the Straits of Malacca and Singapore using Automatic Identification System (AIS) Data, J. Mek., 36(2) [online] Available from: https://jurnalmekanikal.utm.my/index.php/jurnalmekanikal/article/view/58 (Accessed 23 August 2019), 2013.

Sueper, D.: ToF-AMS Analysis Software. Available at, [online] Available from: http://cires1.colorado.edu/jimenez-group/ToFAMSResources/ToFSoftware/index.html., 2015.

Sun, Y., Wang, Z., Dong, H., Yang, T., Li, J., Pan, X., Chen, P. and Jayne, J. T.: Characterization of summer organic and inorganic aerosols in Beijing, China with an Aerosol Chemical Speciation Monitor, Atmos. Environ., 51(0), 250–259, doi:10.1016/j.atmosenv.2012.01.013, 2012.

Sun, Y.-L., Zhang, Q., Schwab, J. J., Demerjian, K. L., Chen, W.-N., Bae, M.-S., Hung, H.-M., Hogrefe, O., Frank, B., Rattigan, O. V. and Lin, Y.-C.: Characterization of the sources and processes of organic and inorganic aerosols in New York city with a high-resolution time-of-flight aerosol mass apectrometer, Atmospheric Chem. Phys., 11(4), 1581–1602, doi:https://doi.org/10.5194/acp-11-1581-2011, 2011.

Ulbrich, I. M., Canagaratna, M. R., Zhang, Q., Worsnop, D. R. and Jimenez, J. L.: Interpretation of organic components from Positive Matrix Factorization of aerosol mass spectrometric data, Atmospheric Chem. Phys., 9(9), 2891–2918, doi:10.5194/acp-9-2891-2009, 2009.

UN Environment: The South East Asia Air Quality Regional Report, UN Environ. [online] Available from: http://www.unenvironment.org/resources/report/south-east-asia-air-quality-regional-report (Accessed 20 March 2019), 2014.

Vander Wal, R. L. and Tomasek, A. J.: Soot nanostructure: dependence upon synthesis conditions, Combust. Flame, 136(1), 129–140, doi:10.1016/j.combustflame.2003.09.008, 2004.

Velasco, E. and Roth, M.: Review of Singapore's air quality and greenhouse gas emissions: Current situation and opportunities, J. Air Waste Manag. Assoc., 62(6), 625–641, doi:10.1080/10962247.2012.666513, 2012.

Viana, M., López, J. M., Querol, X., Alastuey, A., García-Gacio, D., Blanco-Heras, G., López-Mahía, P., Piñeiro-Iglesias, M., Sanz, M. J., Sanz, F., Chi, X. and Maenhaut, W.: Tracers and impact of open burning of rice straw residues on PM in Eastern Spain, Atmos. Environ., 42(8), 1941–1957, doi:10.1016/j.atmosenv.2007.11.012, 2008.

Wang, J., Wu, Y., Ge, X., Shen, Y., Ge, S. and Chen, M.: Characteristics and sources of ambient refractory black carbon aerosols: Insights from soot particle aerosol mass spectrometer, Atmos. Environ., 185, 147–152, doi:10.1016/j.atmosenv.2018.05.011, 2018.

Willis, M. D., Lee, A. K. Y., Onasch, T. B., Fortner, E. C., Williams, L. R., Lambe, A. T., Worsnop, D. R. and Abbatt, J. P. D.: Collection efficiency of the soot-particle aerosol mass spectrometer (SP-AMS) for internally mixed particulate black carbon, Atmos Meas Tech, 7(12), 4507–4516, doi:10.5194/amt-7-4507-2014, 2014.

Willis, M. D., Burkart, J., Thomas, J. L., Köllner, F., Schneider, J., Bozem, H., Hoor, P. M., Aliabadi, A. A., Schulz, H., Herber, A. B., Leaitch, W. R. and Abbatt, J. P. D.: Growth of nucleation mode particles in the summertime Arctic: a case study, Atmospheric Chem. Phys., 16(12), 7663–7679, doi:https://doi.org/10.5194/acp-16-7663-2016, 2016.

Wong, J. P. S., Lee, A. K. Y. and Abbatt, J. P. D.: Impacts of Sulfate Seed Acidity and Water Content on Isoprene Secondary Organic Aerosol Formation, Environ. Sci. Technol., 49(22), 13215–13221, doi:10.1021/acs.est.5b02686, 2015.

World Shipping Council: Global Trade: Top 50 World Container Ports, [online] Available from: http://www.worldshipping.org/about-the-industry/global-trade/top-50-world-container-ports (Accessed 1 September 2019), 2019.

Xu, W., Han, T., Du, W., Wang, Q., Chen, C., Zhao, J., Zhang, Y., Li, J., Fu, P., Wang, Z., Worsnop, D. R. and Sun, Y.: Effects of Aqueous-Phase and Photochemical Processing on Secondary Organic Aerosol Formation and Evolution in Beijing, China, Environ. Sci. Technol., 51(2), 762–770, doi:10.1021/acs.est.6b04498, 2017.

Yakubov, M. R., Milordov, D. V., Yakubova, S. G., Borisov, D. N., Ivanov, V. T. and Sinyashin, K. O.: Concentrations of vanadium and nickel and their ratio in heavy oil asphaltenes, Pet. Chem., 56(1), 16–20, doi:10.1134/S0965544116010072, 2016.

Yang, L., Nguyen, D. M., Jia, S., Reid, J. S. and Yu, L. E.: Impacts of biomass burning smoke on the distributions and concentrations of C2–C5 dicarboxylic acids and dicarboxylates in a tropical urban environment, Atmos. Environ., 78, 211–218, doi:10.1016/j.atmosenv.2012.03.049, 2013.

Zhang, Q., Worsnop, D. R., Canagaratna, M. R. and Jimenez, J. L.: Hydrocarbon-like and oxygenated organic aerosols in Pittsburgh: insights into sources and processes of organic aerosols, Atmospheric Chem. Phys., 5(12), 3289–3311, doi:10.5194/acp-5-3289-2005, 2005.

Zhang, Q., Jimenez, J. L., Worsnop, D. R. and Canagaratna, M.: A Case Study of Urban Particle Acidity and Its Influence on Secondary Organic Aerosol, Environ. Sci. Technol., 41(9), 3213–3219, doi:10.1021/es061812j, 2007a.

Zhang, Q., Jimenez, J. L., Canagaratna, M. R., Allan, J. D., Coe, H., Ulbrich, I., Alfarra, M. R., Takami, A., Middlebrook, A. M., Sun, Y. L., Dzepina, K., Dunlea, E., Docherty, K., DeCarlo, P. F., Salcedo, D., Onasch, T., Jayne, J. T., Miyoshi, T., Shimono, A., Hatakeyama, S., Takegawa, N., Kondo, Y., Schneider, J., Drewnick, F., Borrmann, S., Weimer, S., Demerjian, K., Williams, P., Bower, K., Bahreini, R., Cottrell, L., Griffin, R. J., Rautiainen, J., Sun, J. Y., Zhang, Y. M. and Worsnop, D. R.: Ubiquity and dominance of oxygenated species in organic aerosols in anthropogenically-influenced Northern Hemisphere midlatitudes, Geophys. Res. Lett., 34(13), L13801, doi:10.1029/2007GL029979, 2007b.

Zhang, Q., Jimenez, J. L., Canagaratna, M. R., Ulbrich, I. M., Ng, N. L., Worsnop, D. R. and Sun, Y.: Understanding atmospheric organic aerosols via factor analysis of aerosol mass spectrometry: a review, Anal. Bioanal. Chem., 401(10), 3045–3067, doi:10.1007/s00216-011-5355-y, 2011.

Table 1: Top: Carbon fragment ratios observed by the laser-on measurement for each PMF factor. The underlined number represents the results with both rBC fragments and trace metal ions included as PMF input. Bottom: Contribution of each PMF factor to the total signal of specific metal ions. For the entire table, the values in parenthesis are the one obtained from PMF with CDCE-corrected input matrix (see details in Text S1 and Table S4 of the supplementary information).

PMF factors	**HOA**	**O-HOA**	**COA**	**LO-OOA**	**MO-OOA**
Carbon fragments ratios					
C_1^+/C_3^+	0.66 (0.63) 0.65 (0.62)	1.00 (0.90) 1.00 (0.89)	NA*	0.81 (0.88) 0.79 (0.85)	NA#
C_2^+/C_3^+	0.38 (0.39) 0.38 (0.39)	0.41 (0.40) 0.41 (0.40)	NA*	0.39 (0.41) 0.41 (0.40)	NA#
Contribution of each factor to the total signal of specific metal ions (fraction)					
Na^+	0.35 (0.22)	0.14 (0.17)	< 0.01 (< 0.01)	0.45 (0.58)	0.06 (0.03)
K^+	0.23 (0.23)	0.19 (0.18)	< 0.01 (< 0.01)	<0.01 (0.05)	0.58 (0.54)
V^+	0.21 (0.08)	0.09 (0.16)	< 0.01 (< 0.01)	0.70 (0.76)	< 0.01 (< 0.01)
Ni^+	0.38 (0.22)	0.20 (0.22)	< 0.01 (< 0.01)	0.29 (0.45)	0.13 (0.11)
Rb^+	0.15 (0.15)	0.19 (0.19)	< 0.01 (< 0.01)	<0.01 (0.01)	0.66 (0.65)

* None of the refractory C_n^+ fragments were associated with the COA factor

Large variations of C_n^+ fragment ratios between cases, hence the ratios were not reported for MO-OOA

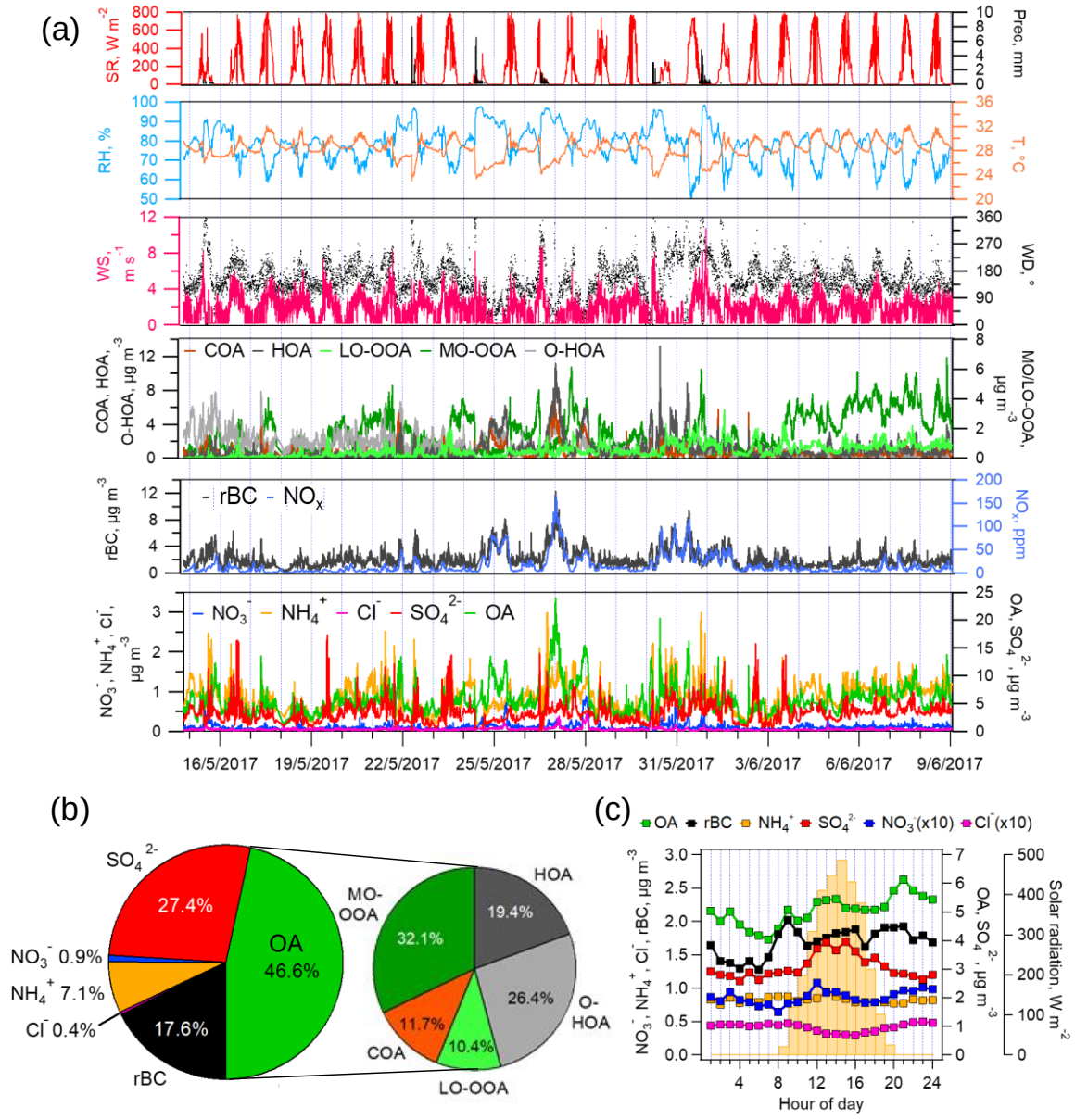

Figure 1: (a) Time series of solar radiation (SR), precipitation, temperature, relative humidity, wind speed (WS) and direction (WD), PMF factors (HOA, O-HOA, COA, LO-OOA, and MO-OOA from laser-off measurements), rBC, NO_X, total OA and inorganic species. (b) Average chemical compositions of NR-PM and rBC with the contribution of the PMF factors to total OA. (c) Diurnal patterns of rBC, total OA, inorganic species and solar radiations (represented by the yellow bars).

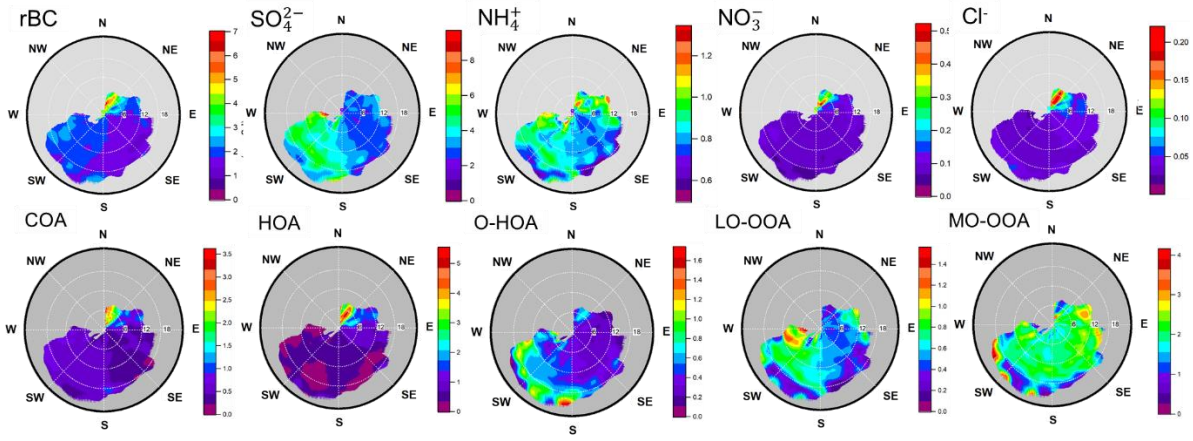

Figure 2: NWR plots of aerosol components measured by the SP-AMS during the whole campaign (Note: all species and OA components are from laser-off measurements except for rBC).

5

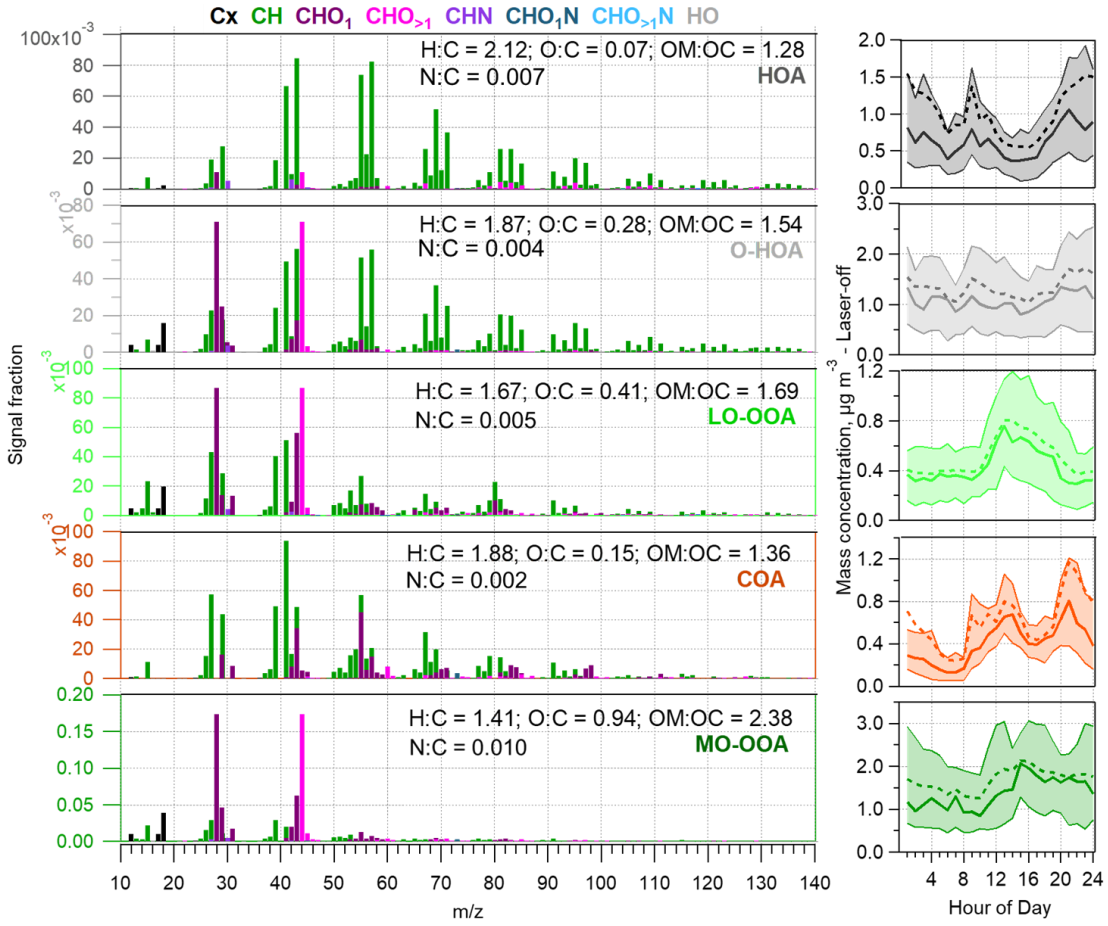

Figure 3: (Left) Mass spectra and elemental ratios of the five-factor solution obtained from the PMF analysis of laser-off measurements and (right) their respective diurnal cycles (median - plain line, mean – dotted line, 25th and 75th centiles - shaded area) for the entire campaign. The PMF results from laser-on measurements are shown in Figure S4.

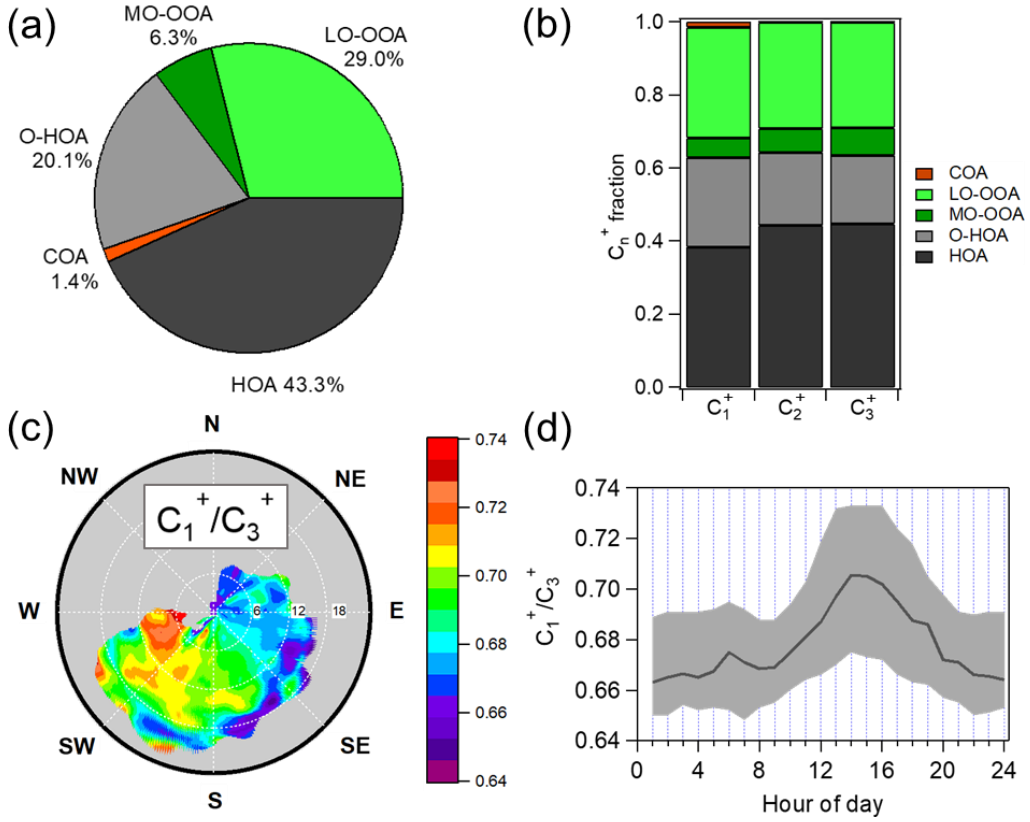

Figure 4: (a) Fractions of rBC and (b) relative contributions of C_1^+-C_3^+ fragments contributed by the five OA components identified by the PMF analysis with OA and rBC fragments measured by the laser-on mode as model inputs. (c) NWR plot and (d) diurnal cycle of C_1^+/C_3^+ ratio (25^{th} and 75^{th} centiles - shaded area).

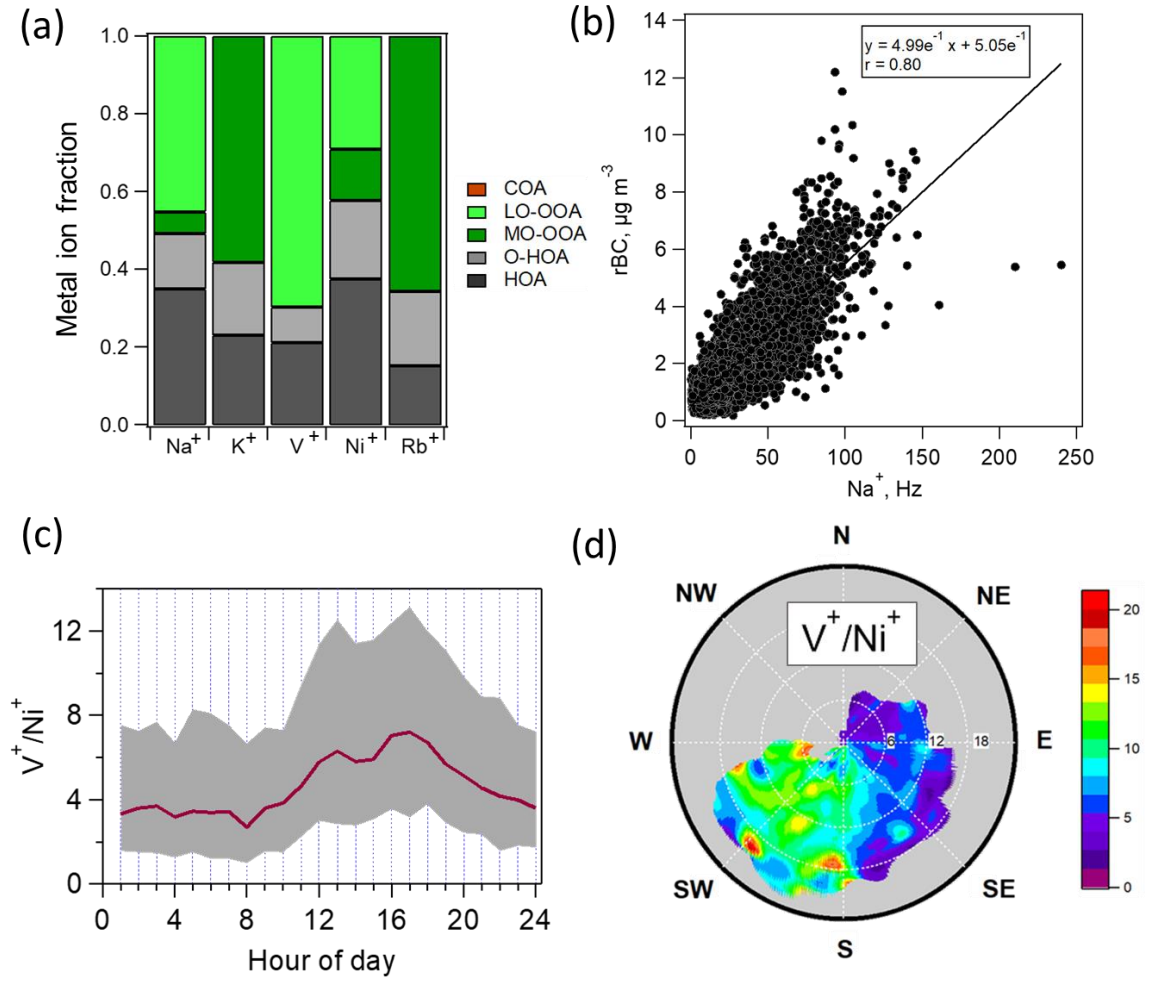

Figure 5: (a) Fractions of trace metal ions contributed by each OA component obtained from the PMF analysis with OA, rBC, and metal ions measured by the laser-on mode as model inputs. (b) Scatter plot of 5-min averaged rBC concentrations vs. Na^+ signals. (c) Diurnal cycle of V^+/Ni^+ ratio (25^{th} and 75^{th} centiles - shaded area). (d) NWR plot of V^+/Ni^+ ratio over the entire campaign.

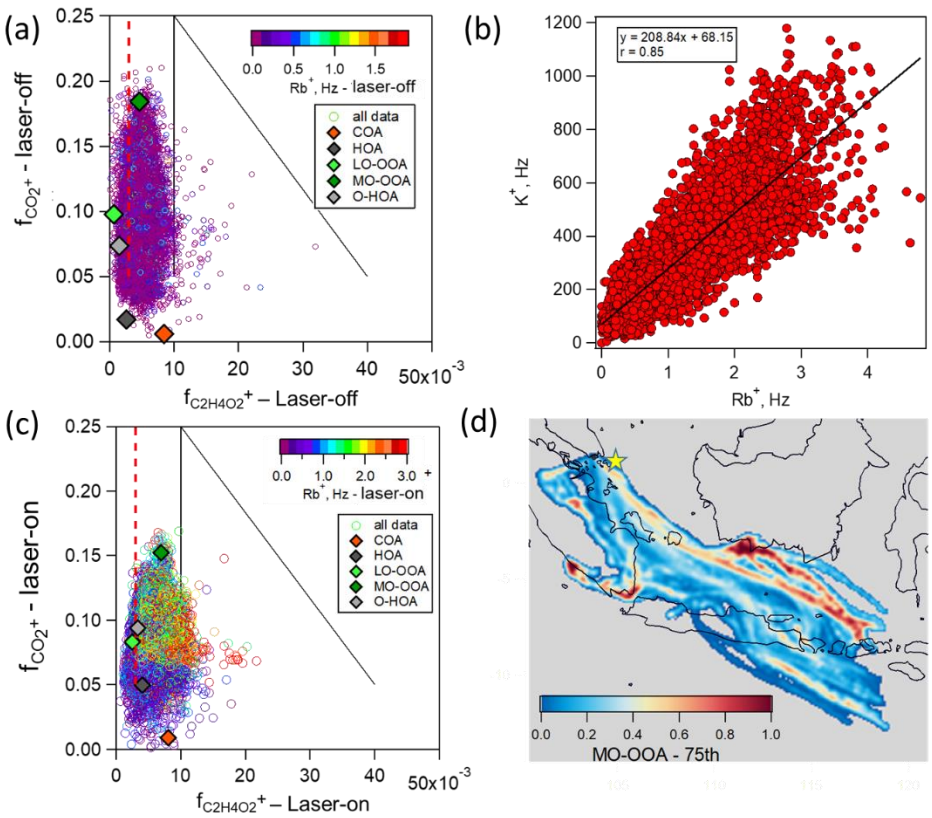

Figure 6: Scatter plots of f_{CO2+} vs. $f_{C2H4O2+}$ with the symbol color scaled by the rubidium (Rb^+) ion signals based on (a) laser-off and (c) laser-on measurements (Dash red line – 0.3% background value, plain black lines define the space with and without BB influence (inside and outside the triangular region, respectively, Cubison et al., (2011)). (b) Scatter plot of potassium ion (K^+) vs. rubidium (Rb^+) signals from the laser-on measurements. (d) PSCF graph of MO-OOA by considering only pollutant concentrations above their respective 75th percentile (Figure S15 shows PSCF graphs of K^+, Rb^+, and $C_2H_4O_2^+$)